Universidade de Aveiro
Departamento de Eletrónica, Telecomunicações e Informática
2017

Pedro Alexandre Armas Camacho

Desenvolvimento de 'Front-End' para Sistemas de Comunicação por Luz Visível

Front-End Design for Visible Light Communications Systems

Universidade de Aveiro
2017

Departamento de Eletrónica,
Telecomunicações e Informática

Pedro Alexandre Armas Camacho

Desenvolvimento de 'Front-End' para Sistemas de Comunicação por Luz Visível

Front-End Design for Visible Light Communications Systems

Dissertação apresentada à Universidade de Aveiro para cumprimento dos requisitos necessários à obtenção do grau de Mestre em Engenharia Electrónica e Telecomunicações, realizada sob a orientação científica do Doutor José Luís Vieira Cura, Professor Auxiliar do Departamento de Eletrónica, Telecomunicações e Informática da Universidade de Aveiro, e da Doutora Mónica Jorge Carvalho Figueiredo, Professora Adjunta do Departamento de Engenharia Electrotécnica da Escola Superior de Tecnologia e Gestão de Leiria.

Dedico este trabalho à minha mãe, por tudo.

o júri / the jury

presidente / president

Prof. Doutor Paulo Bacelar Reis Pedreiras
professor auxiliar da Universidade de Aveiro

vogais / examiners committee

Prof. Doutor Nuno Miguel Ferreira Miranda
professor adjunto do Departamento de Engenharia Eletrotécnica da Escola Superior de Tecnologia e Gestão do Instituto Politécnico de Leiria

Prof. Doutora Mónica Jorge Carvalho Figueiredo
professora adjunta do Departamento de Engenharia Eletrotécnica da Escola Superior de Tecnologia e Gestão do Instituto Politécnico de Leiria

agradecimentos /
acknowledgements

Tendo finalizado esta etapa na minha vida, resta-me agradecer a todos os que de alguma forma contribuíram para este trabalho, e a quem me apoiou durante este percurso académico.

À Universidade de Aveiro e Instituto de Telecomunicações de Aveiro manifesto o meu apreço pela possibilidade de realização do presente trabalho, e por todos os meios colocados à disposição, assim como a excelência de formação prestada e conhecimentos transmitidos, ambicionando que o trabalho desenvolvido dignifique ambas as instituições.

Aos orientadores desta dissertação, Professor José Luís Vieira Cura e Professora Mónica Jorge Carvalho Figueiredo por toda a atenção, disponibilidade, e também por todos os conhecimentos transmitido. Deixo também um especial agradecimento ao Professor Luís Filipe Mesquita Nero Moreira Alves, que também me acompanhou ao longo deste trabalho e, e cujo o contributo foi fundamental para a concretização do mesmo.

A todos os meus colegas de laboratório, que de alguma forma contribuíram para o desenvolvimento deste trabalho, deixando um especialíssimo agradecimento para o meu colega Luís Filipe Abade Rodrigues, que foi o meu principal apoio durante a realização dos trabalhos para esta dissertação.

À minha mãe, Graça, que nunca desistiu de mim, e a quem devo tudo. Ao meu pai, Luís Paulo, e ao meu avô, Rui, que infelizmente não me puderam ver chegar aqui. À minha irmã, Paula, ao meu cunhado Fábio, e a todos os restantes familiares, e amigos, que de alguma forma me apoiaram.

Por fim um muito especial agradecimento do fundo do coração ao Flávio Meneses e á Sara Faria que me aturaram nestes últimos meses e que me acolheram como família.

A todos, muito obrigado.

Palavras Chave VLC, LED, Driver, Redes Sem Fios.

Resumo

As Telecomunicações são fundamentais nos nossos dias em que tudo está interligado, levando as tecnologias de telecomunicações constantemente ao seu limite. Todo o tipo de melhoria que possa ser feito para melhorar o desempenho de uma rede, encontrará aplicação em alguma área, mais específica, ou caso se justifique, até mesmo em tecnologias de telecomunicação mais comuns. Um exemplo é o VLC (Visible Light Communication), que pode ser utilizado para melhorar as capacidades de outros tipos de redes de telecomunicações, ou em alternativa a outros tipos de redes, oferecendo vantagens em certos cenários onde métodos tradicionais de telecomunicações sem fios não teriam tão bom desempenho, ou não serviriam a aplicação desejada. O VLC também tem como grande vantagem a hipótese de utilização de um novo meio de transmissão para sistemas de telecomunicações, que é o espectro da luz vísivel, que não se encontra ainda sobrelotado e tem regulamentos mais relaxados que outros meios de comunicação tradicionais. Este trabalho foi feito em colaboração com o grupo de sistemas e circuitos integrados do Instituto de Telecomunicações Aveiro, e visa o estudo de desenvolvimento de 'front ends' óticos para VLC, para utilização futura em projetos por parte deste grupo.

Keywords VLC, LED, Driver, Wireless Networks.

Abstract

Communications are vital in the world today. Everything is connected and this means that communication technologies are constantly being pushed to their limits. Any kind of development and improvement that can be done to increase networks capabilities, will find use in some specific application, or even in more common technologies if such is justified. One such case is VLC, it can be used to improve other communication methods capabilities, or as standalone solution, providing advantage in certain scenarios where regular wireless communications methods would not perform as well, or would not suit the application. VLC also offers the great advantage of utilising a new medium of transmission for telecomunication systems, which is the visible light spectrum, and is not yet overused and overregulated as other typical mediums. This work was done in partnership with the integrated circuit systems groupd of Instituto de Telecomunicações Aveiro and aims to study and develop optical front end systems for VLC to be used in future projects by this group.

Contents

List of Figures

List of Tables

Acronyms

APD	Avalance Photo Diode
BW	Bandwidth
CMRR	Common-Mode Rejection Ratio
DUT	Device Under Test
EM	Electromagnectic
FOV	Field of View
FFT	Fast Fourier Transform
HB	High Brightness
InGaN	Indium Gallium Nitride
IoT	Internet of Things
IR	Infrared
LED	Light Emmiting Diode
LOS	Line-of-sight
VLC	Visible Light Communication
OWC	Optical Wireless Communication
OOK	On-Off Keying
OFDM	Orthogonal Frequency-Division Multiplexing
pc-LED	Phosphor Converted LED
PD	Photodetector
PCB	Printed Circuit Board
RF	Radio Frequency
SiC	Silicon Carbide

CHAPTER 1

Introduction

In this era of continuously evolving technologies that we live in, when everything needs to be connected, networking capability has become a requisite in almost every electronic device. As such we've reached a point where human beings are not the only users of networks anymore, and a lot of devices are constantly communicating with each other autonomously in what is now called Internet of Things (IoT), generating massive amounts of connections and data transfer, which in turns has created new challenges to existing network infrastructures. Some of these challenges may be of network management nature, data capacity, computing capacity or communication channel capacity. Though modern communication channels are in continuous evolution, and being regularly updated, there are applications where one method of communication may have to be complemented with another medium of transmission in order to achieve a specific goal, or to overcome capacity limitations. Many times physical line methods are combined wireless to achieve BW and coverage requirements, such as in a work or home networks.

Predominately, wireless technologies have been Radio Frequency (RF) or Infrared (IR) based, but with advancements of Light Emmiting Diode (LED) technology that made LED's a common illumination source, a new medium of communication known as Visible Light Communication (VLC) has become a possibility. This new technology can be seen as a solution for some shortcomings of traditional wireless technologies, such as spectrum allocation limitations, power constraints, security, and can also offer new capabilities not seen before.

The main goal of this work is to create a driver capable of actuating a High Brightness (HB) LED and modulate its luminosity in order to establish an effective communication channel.

1.1 Motivation

New HB LED's are becoming more common each day as a mean of efficient illumination. They are now present in almost every form of lighting system used, traffic signs, car headlights, flashlights, street lights and home illumination. With other improvements made in HB LED's and this omnipresence they have become potential hosts for other uses, such as communication.

When integrated with other types of communication infrastructure they could become very efficient in different ways, such as RF spectrum relief, power efficiency, low interference, security, spatial location and more.

Some study groups such as the hOME Gigabit Access project (OMEGA) [1], have been created to promote the advantages VLC systems offer in current and future telecommunication scenarios, and to improve these systems technological capabilities.

1.2 Context

This work was developed for the VLCLighting project, a collaborative resarch project developed at Instituto de Telecomunicações Aveiro, that aimed to develop public illumination systems with integrated communication capabilities. The aim of this work is to develop and study a possible optical front end layer system for this project.

1.3 Methodology

The development of this thesis was based on research of previous similar projects upon which goals and requirements were set for the hardware to be developed, all circuits were designed to meet these standards. The second step was to study the LED properties and frequency response in order to simulate all circuits effectively. Finally all systems were mounted on PCB, tested and measured to obtain experimental circuits operation results.

1.4 Dissertation Structure

This disseration is composed of five chapters. This is a brief description of the information present on eache one.

- Chapter one provides a brief introduction to the work developed. It describes the technological context and the main objective and methods used. Also presents a list of contributions done during the project.
- Chapter two compiles a state of the art of VLC with references to its history, methods of implementation, LED types and commonly used components for VLC drivers.
- Chapter three describes the procedure of designing the VLC driver. Here all schematics are shown, and predictions of gain, BW and other parameters values are calculated.
- Chapter four provides all the measurements done for this work on the prototype implemented. Also some conclusions about the experimental results are done here.
- Chapter five comprises the resumed conclusion and plans for future work.

1.5 Contributions

This work contributed with research for two papers. The first one titled "Thermal analysis of high power LEDs", for the conference "Workshop on Compound Semiconductor Devices and Integrated Circuits held in Europe" [2], and the other titled Thermal "Analysis of high power LEDs using different PCB materials ", for the "European Conference on Circuit Theory and Design" [3].

CHAPTER 2

Visible Light Communication

VLC is an Optical Wireless Communication (OWC) field which relies on modern LED modulation capabilities to transmit information over the visible the light spectrum. It shares some working resemblance to its counterpart, IR communication, which uses the IR spectrum as a communication medium. VLC can be seen either as an alternative to other wireless technologies, such as RF communications, or as a complement for other wired and/or wireless technologies, addressing shortcomings of coverage, Bandwidth (BW), efficiency and security [4], that other types of communication methods might have. VLC can also be used for localization [5] and other specific purposes.

This chapter presents a study on the state of the art of VLC technologies. It includes a brief history of OWC and how VLC came to be considered as an alternative, and it also includes a study of relevant methods for circuits design and suited components.

2.1 Optical Wireless Communications History

Historically, human beings have been using optical communication for a long time. Since the early use of smoke signals by native Americans, to ship signal lamps, which used Morse code to transmit information. Optical communications have been present, in different forms, throughout history.

The first known use of visible light as a medium of communication comes from Alexander Graham Bell, with the invention of the photophone, which used beams of sunlight to transmit voice data. [6]

The most common used medium for wireless data transmission systems has been the RF spectrum, which over the years, became over-populated and over-regulated, leading to increased costs of use and strict BW limitations. These can be addressed by the usage of other bands of the Electromagnectic (EM) spectrum, which are not so commonly used for data communication systems.

Optical communications are already a very common method of communication nowadays, however the more advanced and used technologies are optical fibers, and IR. The first being

used for massive data transmission with large BW, but has the downside of needing the physical connection of an optical fiber, and the latter being usually used for small distances and low data rate transmissions, like remote control links.

VLC systems operate in the visible light spectrum, which unlike the IR and RF spectrum have more relaxed rules and regulation in terms of safety and capacity. While IR and RF communications have power constraints, due to health safety regulations, the same does not apply to the visible light spectrum, which can safely use higher power levels for communication transmission and lighting purposes. The visible light spectrum also has the benefit of being less crowded, meaning that most wave lengths are free to use without previous band allocations, additional licensing or BW limitations. This contrasts with the RF spectrum which is under heavy usage and has most of its bands already allocated and regulated for other purposes.

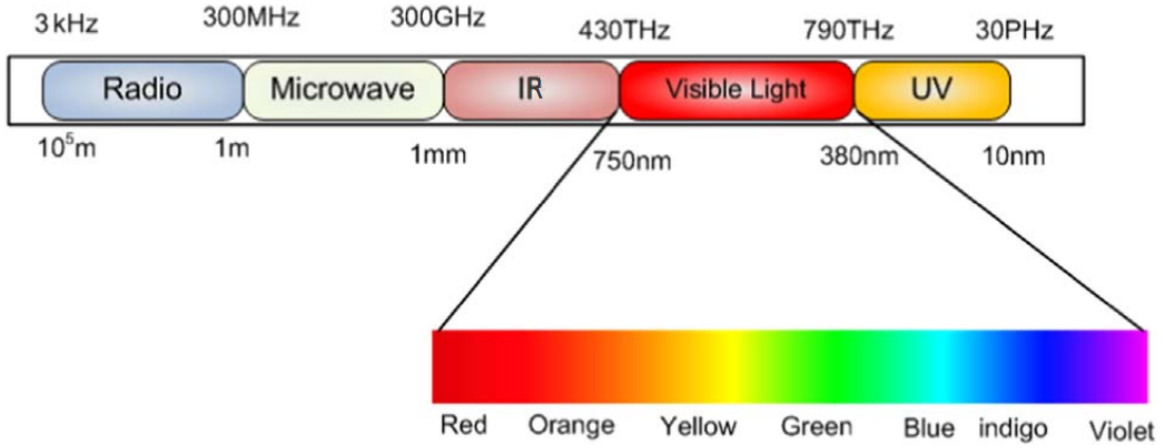

Figure 2.1: Electro Magnetic spectrum and wavelength allocation [7]

2.1.1 VLC Technological Context

VLC became possible due to recent advancements in LED technology, since it relies on the fast switching capability of LEDs in order to modulate its intensity. This, combined with the improvements in efficiency that made LEDs capable of high illumination levels, paved the way for VLC to be an effective alternative method of wireless communication, with early examples being applied to traffic signaling in 1993 [8].

With these advancements some groups were formed to study and promote VLC technology and standards, like the Visible Light Communication Consortium (VLCC), and the hOME Gigabit Access project (OMEGA) which intended to provide gigabit access VLC connections for home users. Also the first IEEE standard for VLC was announced in 2011, the IEEE 802.15.7-2011.

A simple description of a common VLC system can be seen in Figure 2.2. Here we can see that the LED and Photodetector (PD) blocks are present both in the optical and electrical domain since they are the elements of this system responsible to convert electrical signals into optical signals and vice versa.

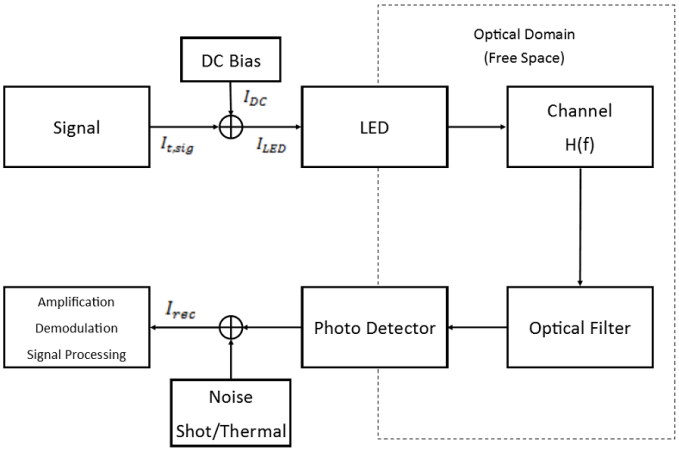

Figure 2.2: VLC system block diagram

2.2 Physical Components

2.2.1 Light Emmiting Diodes

LEDs first appeared in the early 20^{th} century [9], with the use of Silicon Carbide (SiC) crystallites and II-VI semiconductors as light emitting materials, which prevailed has the main used material until the 1950's. SiC and some II-VI semiconductors occur in nature.

In 1952 Heinrich Welker filed a patent for the first III-V compound semiconductor [10], these compounds, which do not occur naturally, proved instrumental in the development of modern LED technologies, since they shown to be optically very active. Though this began the advent of the use of synthetic semiconductor compounds for LED fabrication, and gave way to the development of other semiconductor compounds with different properties either of efficiency or color range. In the beginning most LEDs were used for IR and laser applications [11] , and shown external quantum efficiencies of around 6% [12]. These early accomplishments pale in comparison to modern LEDs' efficiencies values, but paved the way for LEDs to become common illumination sources in our days.

Two possible construction methods for LEDs are shown in Figure 2.3. Planar structure LEDs are frequently combined with lenses to focus its light emission pattern. A brief summary of different LED types and their most important properties is presented in table 2.1, and Table 2.2 presents some construction materials according to wavelength generated by the LED.

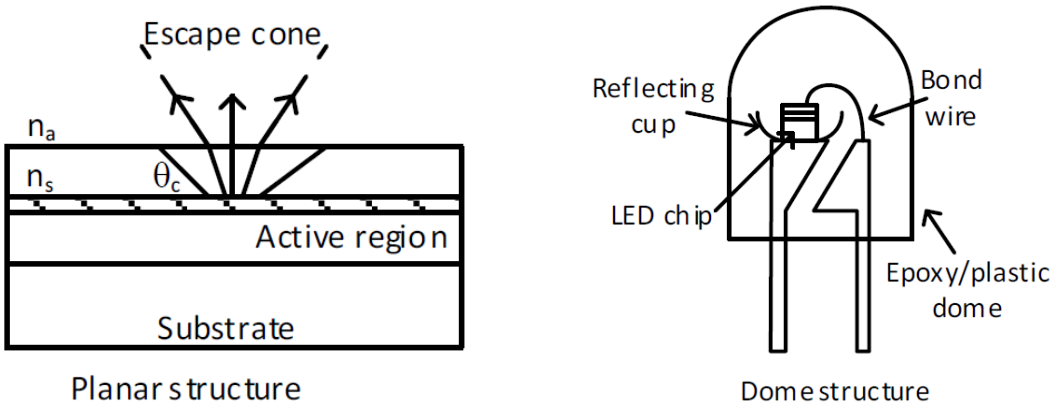

(a) LED planar structure

(b) LED dome structure

Figure 2.3: LED structures [13]

Table 2.1: LED types and common properties [14]

Parameter	**pc-LED**	**RGB LED**	**u-LED**	**OLED**
Bandwidth	3-5 Mhz	10-20 MHz	≥300 MHz	≤1 MHz
Efficacy	130 lm/W	65 lm/W	N/A	45 lm/W
Cost	Low	High	High	Lowest
Complexity	Low	Moderate	Highest	High
Application	Illumination	Illumination	Bio-sensors	Display

High brightness LEDs

High efficiency white LEDs are commonly based on blue Indium Gallium Nitride (InGaN) LEDs which started appearing in the late 1990's and early 2000's, and are also known as Phosphor Converted LED (pc-LED). These white LEDs rely on different wavelength conversion techniques, which take the blue light single wavelength component emission of the InGaN LED and spread it over the visible light spectrum with the use of a phosphor filter layer commonly made of YAG:Ce, yttrium aluminum garnet doped with cerium ions [15], thus creating a multiple wavelength composed white light, as seen on Figure 2.4.

The process of converting the blue light into white on these LEDs is based on the absorption of photons of a given energy by the phosphor coating, that are then re-emitted with a lower energy. The excitation photons, frees valence electrons within the phosphor that undergo a process of non-radiative decay by which they have their energy lowered. Considering the the fact that energy and wavelength are inversely related, a photon with a blue dominant wavelength will be re-emitted as a photon of lesser energy, and larger wavelength, in this case being on the yellow region of the spectrum [13]. However this method of achieving white light radiation comes at a cost, while the blue LED might initially present a BW of 10MHz, the phosphor converting layer will reduce this BW to not much more than 3MHz. This happens due to the phosphorescent material carrier decaying time.

The emitted optical power ($P_{optical}$) can be seen as relation of the total electrical power

($P_{electrical}$) and its power conversion efficiency factor (η_{PCE}).

$$P_{optical} = P_{electrical} \propto \eta_{PCE} \tag{2.1}$$

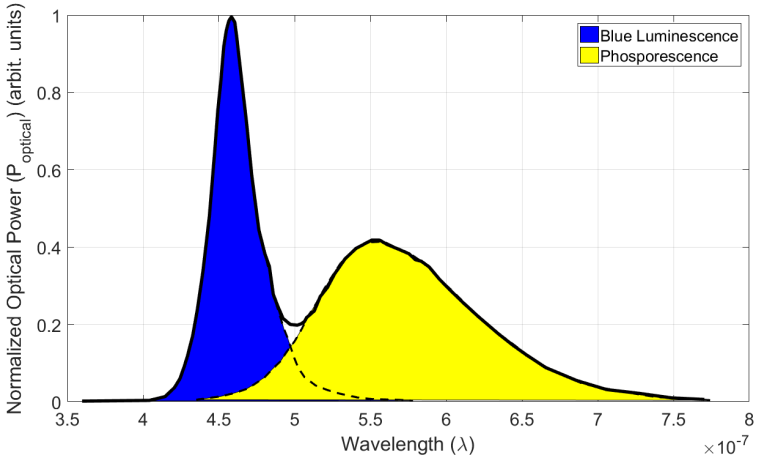

Figure 2.4: pc-LEDs emission spectrum

Table 2.2: LED colors wavelength and common build materials

Color	**Wavelength [nm]**	**Semiconductor material**
Infrared	$\lambda > 760$	GaAs AlGaAs
Red	$610 < \lambda < 760$	AlGaAs GaAsP AlGaInP GaP
Orange	$590 < \lambda < 610$	GaAsP AlGaInP GaP
Yellow	$570 < \lambda < 590$	GaAsP AlGaInP GaP
Green	$500 < \lambda < 570$	GaP AlGaInP AlGaP InGaN / GaN
Blue	$450 < \lambda < 500$	ZnSe InGaN
Violet	$400 < \Delta V < 450$	InGaN
Purple	Multiple types	Dual blue/red LEDs blue with red phosphor or white with purple plastic
Ultraviolet	$\lambda < 400$	InGaN Diamond Boron nitride AlN AlGaN AlGaInN
Pink	Multiple types	
White	Broad Spectrum	Cool / Pure White: Blue/UV diode with yellow phosphor Warm White: Blue diode with orange phosphor

2.2.2 Photodetectors

A PD is a device capable of detecting light or other electromagnetic energy. Though there are different types of PD's classified by the mechanism used to detect photons, due to their properties photodiodes are predominantly the choice used in VLC. These photodiodes usually rely on p-n junctions to convert incident photons into electrical current, and are similar to LEDs, being built with some of the same semiconductor compounds as LEDs, but working on reverse current bias mode.

The ideal PD should be able to detect all incident photons, respond to the fastest received signal changes of interest, and should not introduce shot-noise beyond the inherent quantum shot-noise of the received signal. Unfortunately, real world PD's are far from perfect, they have limited BW and induce noise in the received signal. [16]

Though PD's detection capability is directly proportional to its effective area, larger PD's have some drawbacks, like increased junction capacitance, lower receiver BW, worse noise performance and higher manufacturing costs.

APD

One of the most common used photodiode type in VLC, is the Avalance Photo Diode (APD). It offer higher gains, and seem to perform better in low optical power conditions [17], but it also induces undesired excess shot noise caused by the higher photocurrent [18].

PIN

Another commonly used type of photodiode in VLC is the PIN , which is a variation of the p-n junction photodiode, and is constructed with an intrinsic semiconductor 'i' layer sandwiched between two doped 'p' and 'n' type layers. This kind of PD offer a few advantages over the APD in the VLC context since they have higher temperature tolerances, are less expensive, and seem to perform better under higher illumination scenarios [14].

The incident optical power ($P_{optical}$) can be seen as the relation of the total current generated (I_M) in the PD and its responsivity for each wavelength, as is given by. [13]

$$I_M = P_{optical} \times \Re(\lambda) \tag{2.2}$$

Figure 2.5 shows the relative responsivity curves across the spectrum for 'PIN' PDs with different construction materials.

A brief summary and comparison of different PD types and their properties is listed in table 2.3.

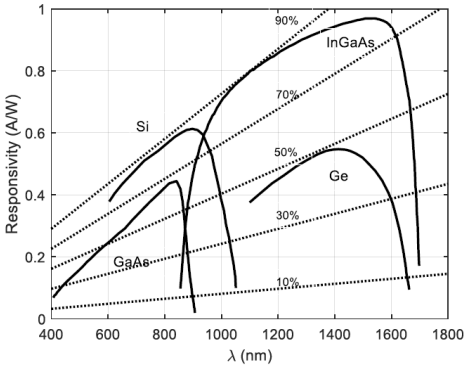

Figure 2.5: Common photodiodes responsivity curves [13]

Table 2.3: Photodetector Characteristics Summary [16]

	Si PIN	Si APD	Ge APD	InGaAs PIN	InGaAsA PD
Useful λ region (nm)	400 - 1150 nm	400 - 1150 nm	800 - 1750 nm	900 - 1700 nm	900 - 1700 nm
QE	60 - 90%	70 - 80%	50 - 80%	70 - 90%	60 - 90%
Gain	1	50 - 300	10 - 100	1	10 - 40
Carrier Ionization Rate (K_{eff})	-	0.01-0.10	0.6-0.9	-	0.2-0.5
Unmultiplied Dark-current (nA)	1 nA	0.1 nA	1 - 50 nA	1 - 10 nA	0.5 - 5 nA
Multiplied Dark-current (nA)	-	0.1 - 1 nA	5-100 nA	-	0.5 - 5 nA
Detector Capacitance (pF)	1 - 5 pF	1 - 5 pF	1 - 5 pF	0.2 - 2 pF	0.2 - 2 pF
Response Time (nS)	0.3 - 3 ns	0.5 - 5 ns	0.3 - 3 ns	0.05 - 1 ns	0.1 - 1 ns

2.2.3 Transistors

Though transistors are commonly used in almost every electronic application these days, in the context of VLC drivers we have met some particular challenging requirements. The transistors used in the output stage of the VLC driver must have high power dissipation ratings, high current gain (h_{fe}), and a large enough BW to ensure linearity in the required working range.

An important property to ensure the required BW of the system is the f_T of the transistor, this parameter corresponds to the highest frequency at which the transistor presents a h_{fe} equal to unity, and permits us to know the current gain evolution since the attenuation of h_{fe} follows a curve of 20dB/dec after its cutoff frequency, as seen in Figure 2.6. These requirements make the selection of suited transistors a difficult task, since there are no transistors specifically

designed for VLC applications, and transistors with these specifications tend to have high manufacturing prices that may render a VLC system economically unpractical for common use.

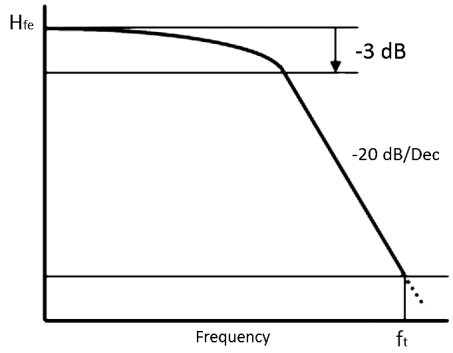

Figure 2.6: Transition frequency

2.3 Optical Source systems

VLC driver design is in itself a challenging task, as it deals with the constrains of two distinct electronic design areas. Since power electronics techniques and components suited to be used with high power LEDs may lead to BW limitations, the BW optimization and linearity of the system becomes compromised.

For VLC, two types of driver can be defined according to their modulation capabilities, "On-Off" and analog drivers. The first being suited for digital transmission formats with single logic levels such as On-Off Keying (OOK), and the latter being used for more complex modulations schemes with continuous or multiple output levels like Orthogonal Frequency-Division Multiplexing (OFDM).

As for the analog control methods, there are also two possibilities to consider. Modulation can be achieved either by direct control of the LED forward current, or by controlling the voltage applied to the LED, indirectly modulating its current [13]. For this work, only analog control methods will be considered, as the driver will be design for analog modulation.

Figure 2.7 and Figure 2.8 present conceptual designs for a voltage control mode and current control mode drivers. The working principles for each one will described in the next subsection.

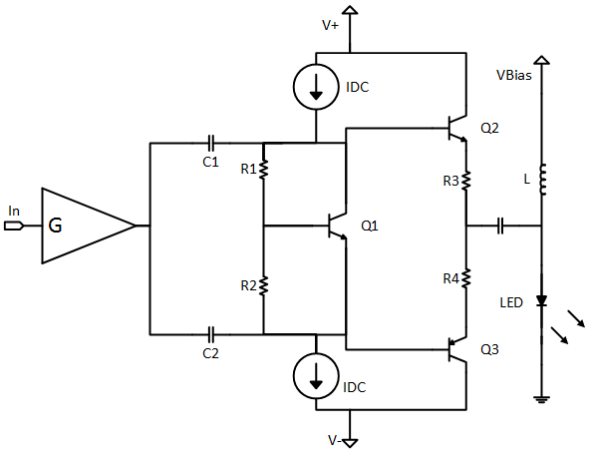

Figure 2.7: Push-Pull conceptual voltage driver

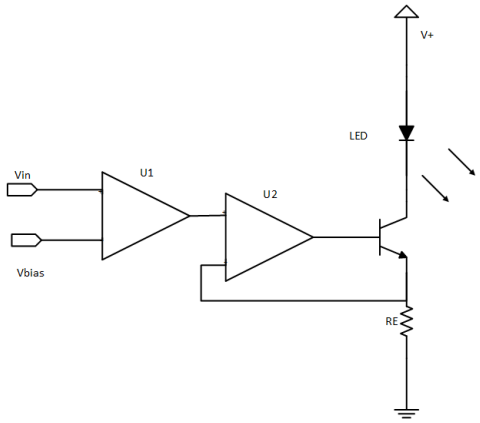

Figure 2.8: Conceptual current driver

2.3.1 Current Mode

Current mode offers the advantage of a close to linear response, since current is being directly altered on the LED without any conversion factors. This mode however, has to deal with heavy power ratings being dissipated on the biasing element for the LED. As can be seen on Figure 2.8, the transistor M1 would be responsible for not only modulating the signal but also for biasing the LED, which would ask for a transistor capable of high power handling, and large BW. These drivers are usually implemented in a transconductance topology in which the output current is directly related to the input voltage.

2.3.2 Voltage Mode

Voltage mode does not offer such a linear response as current mode, but has the advantage of separating the LED biasing from the driver itself. This allows for a wider possibility of components to be used in the driver design, since the signal part of the system will be only required to have a large BW, and not high power handling capabilities. Usually in this mode, biasing of the LED is accomplished with the use of a Bias-T which is a device capable of combining both the external power supply DC current for the LED biasing and the AC signal of the driver, while keeping the DC current from flowing to the driver.

Voltage mode can be implemented with an A or AB output stage. As before there are compromises to be made between these topologies, since class A exhibits superior linearity (Figure 2.9a) over class AB, but lower theoretical maximum efficiency (η), which is the ratio of the power delivered to the load (P_L) over the total power delivered to the system by the power supply (P_{dc}) [19].

$$\eta_A = \frac{P_L}{P_{dc}} \times 100 \tag{2.3}$$

With the efficiency (η) in the case of the class A output stage, with V_o the voltage applied to the load, I the current delivered to the load, V_{CC} the total voltage of the power supply of the system, and R_L the value of the load.

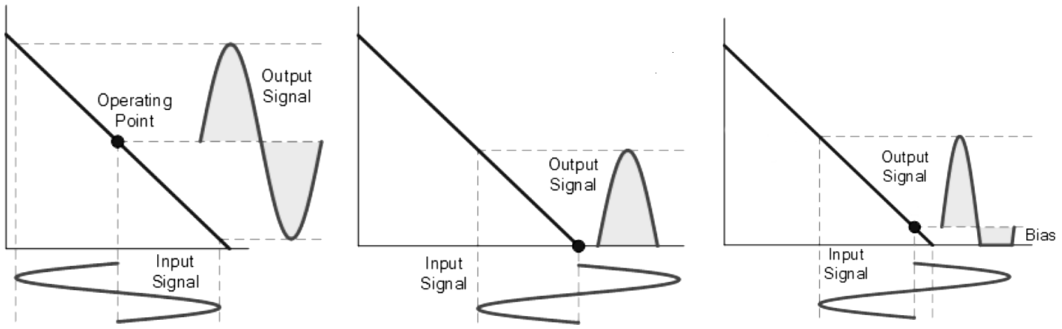

(a) Class A **(b)** Class B **(c)** Class AB

Figure 2.9: Output stages operating curves

$$\eta_A = \frac{1}{4}\left(\frac{V_o}{IR_L}\right)\left(\frac{V_o}{V_{CC}}\right) \tag{2.4}$$

With theoretical maximum efficiency being 25% when.

$$V_o = V_{CC} = IR_L$$

The efficiency (η) of the class AB output stage given by the following equation, with a theoretical maximum efficiency when $V_o = V_{CC}$ of 78%.

$$\eta_{AB} = \frac{\pi}{4}\left(\frac{V_o}{V_{CC}}\right) \tag{2.5}$$

Class AB, works as a compromise between class A and class B, on which DC biasing is added to the input of the transistors, in order to eliminate the cross-over distortion inherent to class B output stages that happens when the signal amplitude is around its middle point and the base voltage (V_{be}) of both transistors is bellow its working threshold (Figure 2.9b). One such example can be seen in Figure 2.7, where a 'VBE multiplier' is used to offset both bases of the output stage in reference to one another, mitigating the dead zone that causes cross-over distortion as seen on figure 2.9c.

2.3.3 Pre-Emphasis

A Pre-Emphasis stage, is a type of preamplifier that boosts predefined frequencies of the signal. Since driving circuits and LEDs have limited BW a pre-emphasis stage can be used to counteract the natural poles caused by the system.

A basic approach to designing a pre-emphasis stage would be using "pole-zero cancellation". For this method, the frequency response of the system to be compensated must be observed and measured in order to determine its pole location, then the pre-emphasis will be designed with a zero appearing at the same frequency of the system pole. The pre-emphasis will then be linked in series with the system to be compensated, creating a flat response of the total system to a higher frequency as its shown in Figure 2.10. A simple conceptual design for a pre-emphasis circuit with two poles is presented in Figure 2.11.

This method is been shown effective to enhance BW in VLC systems up to 143 MHz [20], and when combined with complex modulation techniques resulted in high bit rate capable systems.

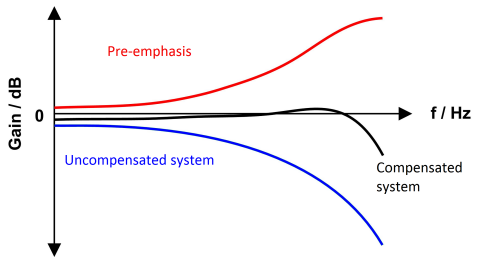

Figure 2.10: Pre-emphasis frequency response

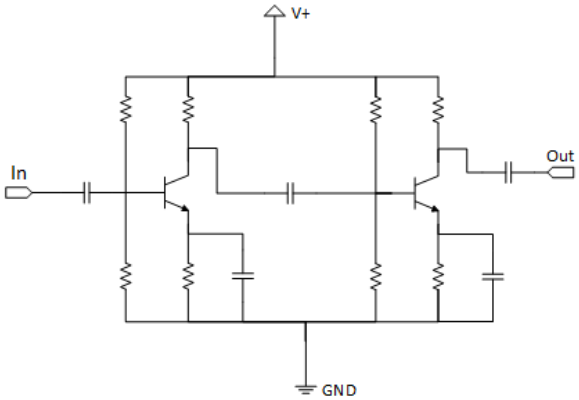

Figure 2.11: Pre-emphasis conceptual voltage driver

2.3.4 DC-signal mixing

When combining DC and AC inputs, a blocking network must be used. The AC signal should not flow to the DC source, and the DC component should never flow to the source. Two possible methods to achieve this are represented in Figure 2.12.

The first, Figure 2.12a, represents a Bias-T approach, in which a device composed of capacitors and inductors called 'Bias-T' lets us connect a DC power supply to the inductor side, which effectively works as a low-pass filter, rejecting the AC signal while still being capable of DC biasing the LED. It also lets us inject the signal through the capacitors which work as high-pass filters, allowing the higher frequencies of the AC signal to pass, while blocking any DC current from flowing to the signal source.

The second, Figure 2.12a, is a more simple approach, relying only on the single capacitor, or a network of capacitors, working as a high-pass filter to block the DC current from flowing to the signal generator, while still allowing the AC signal to be injected. And a simple high power rated resistor connected in series with the LED for biasing purposes.

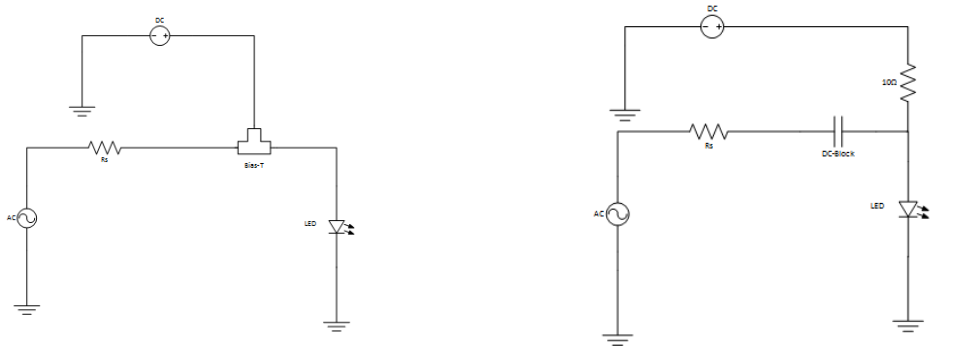

(a) Bias-T biasing

(b) Resistor biasing with DC block

Figure 2.12: Common signal mixing methods

2.4 Optical Detector systems

Optical detector systems are usually designed with a much greater BW than that of the source systems. This is a major requirement to ensure the linearity of the whole communication system, since the receiver must be able to reconstruct the signal without any distortion caused by it's own limitations.

Since photodiodes turn the incident photons directly into current, receiver systems for VLC are usually designed as a transimpedance amplifier, that can sense the current changes in the photodiode, convert them into voltage and amplify them. One example is shown in Figure 2.13.

The choice of PD and amplifier is critical to meet the receiver requirements of BW and noise rejection. Such systems rely on low-noise differential amplifiers capable of high Common-Mode Rejection Ratio (CMRR). Also the PD must have a large enough BW over the transmitter BW, and since VLC works with a range of wavelengths instead of a single wavelength, a responsivity curve that covers the full spectrum of the source emission in order to capture as much optical power as possible. Lenses and filters are also frequently used to improve performance.

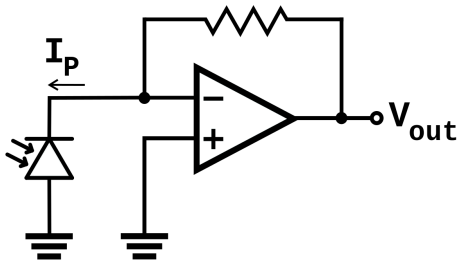

Figure 2.13: Conceptual Transimpedance amplifier for VLC

2.5 Channel Modelling

To describe the propagation of light in the air, we have to take in account the indoor Line-of-sight (LOS) propagation model. [21]

The following equation represents the radiation intensity pattern modelled using a generalized Lambertian radiant intensity distribution.

$$R_0(\Phi) = \begin{cases} \frac{(m_1+1)}{2\pi d^2}\cos^{m_1}(\Phi) & , \quad \text{for } \Phi \in [-\pi/2, \pi/2] \\ 0 & , \quad \text{for } \Phi \in \geq \pi/2 \end{cases} \tag{2.6}$$

m_1 is the Lambert's mode number expressing directivity of the source beam, that is related to LED semiangle at half power ($\Phi_{1/2}$).

$$m_1 = \frac{-\ln(2)}{\ln(\cos(\Phi_{1/2}))} \tag{2.7}$$

Radiant intensity.

$$S(\Phi) = P_t \frac{(m_1+1)}{2\pi}\cos^{m_1}(\Phi) \tag{2.8}$$

$$A_{eff}(\Psi) = \begin{cases} A_r\cos(\Psi) & , \quad 0 \leq \Psi \leq \pi/2 \\ 0 & , \quad \Psi > \pi/2 \end{cases} \tag{2.9}$$

The effective are of the PD is modeled within the angles of Field of View (FOV) with $g(\Psi)$ as the non-imaging concentrator gain, and the trignometric relations represented in Figure 2.14.

$$H_{los}(0) = \begin{cases} \frac{A_r(m_1+1)}{2\pi d^2}\cos^{m_1}(\Phi)T_s(\Psi)g(\Psi)\cos(\Psi) & 0 \leq \Psi \leq \Psi_c \\ 0 & \text{elsewhere} \end{cases} \tag{2.10}$$

The received power.

$$P_{r-los} = H_{los}(0) \cdot P_t \tag{2.11}$$

Refers to a Lambertian transmitter with $m_1 = 1$

$$H_{los}(m_1) = \frac{(m_1+1)}{2} \cdot H_{los} \tag{2.12}$$

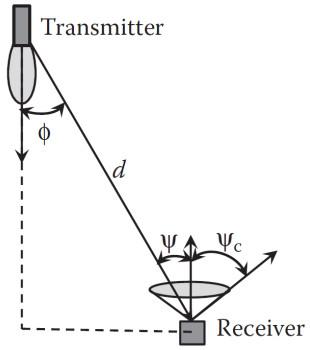

Figure 2.14: Geometry LOS propagation model [21]

CHAPTER 3

System Design

3.1 Driver design

3.1.1 Output stage AB class first iteration

The first iteration of the driver was a simple AB output stage that acted as a current driver and impedance matching network between the signal generator and the biased LED, as shown in Figure 3.1. This circuit was designed as a bipolar amplifier, capable of positive and negative values, operating around 0V and biased by a network of current mirrors to ensure symmetry. The whole system will be powered by a symmetric power supply of -2.5V and +2.5V. This output stage uses a pair of complementary BJT transistors, the 'PBSS4160dpn', to supply the required current gain.

For a gain stage based on a BJT in a common collector configuration, we can determine the gain ($A_v = {}^{v_E}/_{v_B}$) with the help of the small signal 'T' model for the BJT of Figure 3.2. Assuming that only one transistor conducts in each cycle and the output impedance of this stage is the total emitter resistance (R_E) we can assume the following equation of voltage gain.

$$A_v = \frac{R_E + R_{LED}}{r_e + R_E + R_{LED}} \tag{3.1}$$

Our output impedance R_E will be R2 or R3 in series with the LED load, which has been determined to be very low, below 0.5Ω for our operating frequencies. This will be responsible for a very low voltage gain, since $R_E < r_e$, the overall voltage gain of this stage will be smaller than one, approximately 0.25. Table 3.1 presents the values and models of the components used in this circuit.

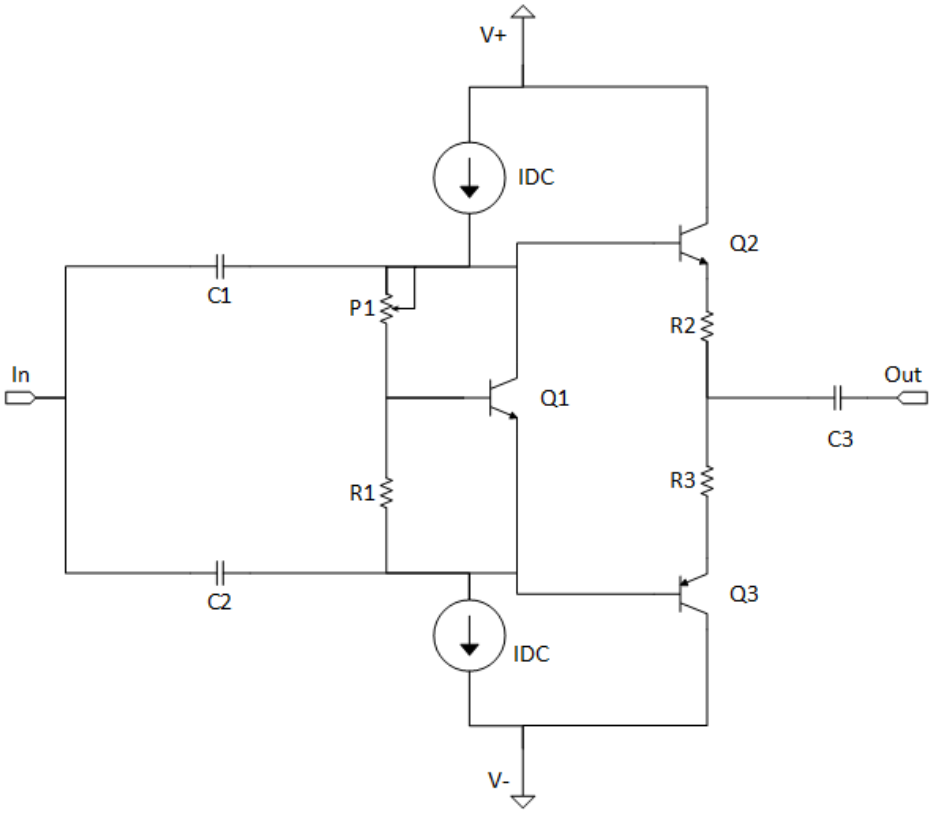

Figure 3.1: AB output stage schematic

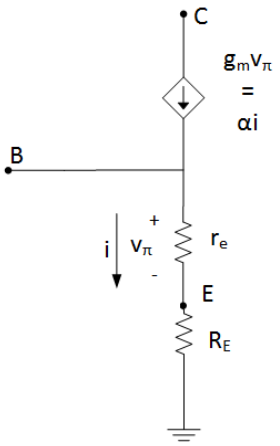

Figure 3.2: BJT small signal T model

Table 3.1: Class AB firt iteration component values

Component	Value/Model
R1	300Ω
R2	0.5Ω
R3	0.5Ω
P1	300Ω
C1	10μF
C2	10μF
C3	10μF
Q1	BFR92A
Q2	PBSS4160dpn - npn
Q3	PBSS4160dpn - pnp
IDC	10mA

3.1.2 Output stage AB class second iteration

To improve the output stage response, and mitigate its voltage attenuating properties a pre-amplifier stage was added. This yielded the second iteration of the output stage, which the schematic is presented in Figure 3.3.

In this version, a two stage amplifier consisting of one stage built with a 'BFR92A' mounted in common emitter configuration, in series with another 'BFR92A' mounted as a common-collector. This system is then connected in series with a AB output stage with a V_{BE} multiplier just like in the first version, but this time with non complementary transistors 'BFG149' and 'BFG19S', which present a higher power rating. With these improvements, the bipolar power supply values for the output stage transistors are now raised to -5V and +5V offering more headroom for the signal.

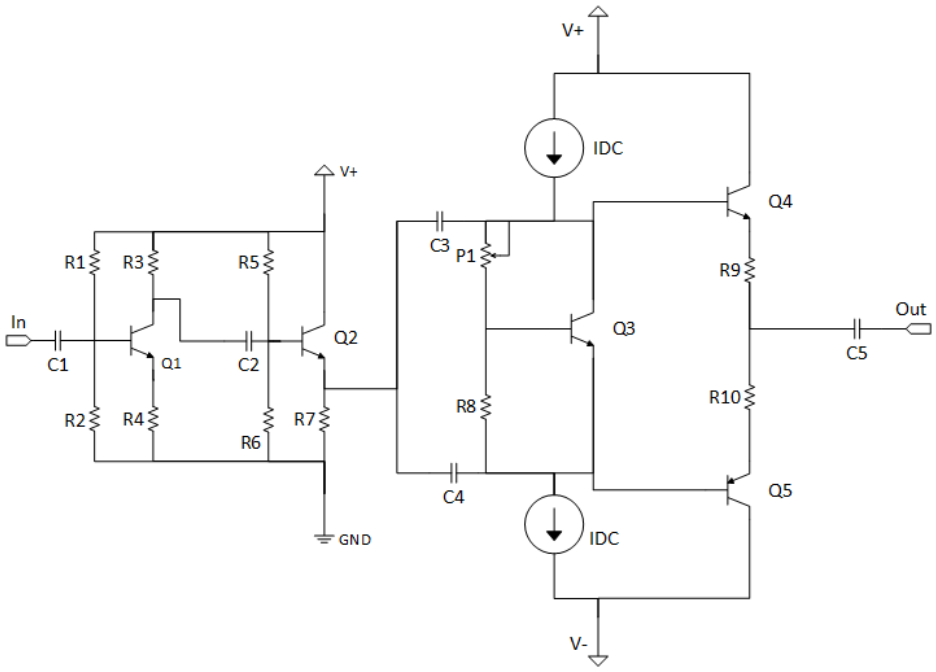

Figure 3.3: AB output stage with pre-amplifier schematic

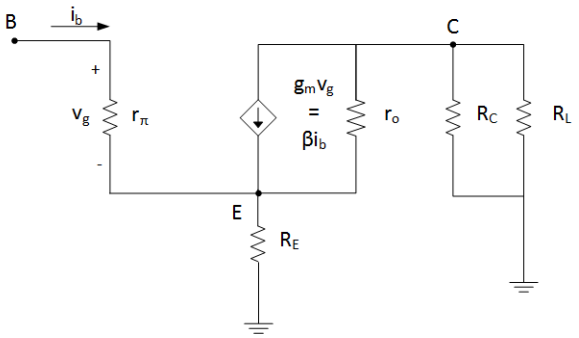

Figure 3.4: BJT small signal pi 'π' model

For a common emitter configuration like the one of the first stage, the gain can be obtained with the help of the small signal model 'π' of Figure 3.4 and the following equation.

$$A_{v1} = -\frac{gm(R_C \parallel R_L)}{1 + gmR_E} \approx -\frac{R_C}{R_E} \tag{3.2}$$

For a common collector like the second stage, we can obtain the gain with the following equation and the help of the small signal model 'T' from Figure 3.2. With the output transistor of the pre-amplifier stage (Q2) capable of driving the output stage, a close to unity gain is expected.

$$A_v = \frac{R_E}{R_E + r_e} \tag{3.3}$$

Now the gain of the full system can be obtained multiplying the gain for the three stages. This will result in an overall negative gain, that will result in an inversion of phase of the signal being transmitted. The first gain stage will be the one responsible for the voltage gain that will nullify the inherent output stage voltage attenuation, and the second stage will be responsible for the necessary current gain, and impedance matching with the output stage. Also of relevance is the use of the capacitor C6 and the resistor R11 which form a high pass filter that gives us the desired signal voltage gain while allowing for adequate biasing of the first stage. Table 3.2 presents the components values and models used for this circuit.

Table 3.2: Class AB second iteration component values

Component	Value/Model	Component	Value/Model	Component	Value/Model
R1	$8k\Omega$	P1	300Ω	Q5	BFQ149
R2	$2k\Omega$	C1	10μF	IDC	10mA
R3	200Ω	C2	10μF	V_1+	10V
R4	100Ω	C3	10μF	V_2+	5V
R5	$7k\Omega$	C4	10μF	V_2-	5V
R6	$3k\Omega$	C5	10μF	-	-
R7	150Ω	Q1	BFR92A	-	-
R8	300Ω	Q2	BFR92A	-	-
R9	0.5Ω	Q3	BFR92A	-	-
R10	0.5Ω	Q4	BFQ19	-	-

The simulation results shown in Figure 3.5 were all obtained using a PSpice simulation software, and were performed using the model of a LED equivalent to the 'Osram Oslon

LCW CR7P' at 350mA current biasing as load. Each curve represents the system response for different input voltage signals from $v_{in} = 50\text{mV}$, to $v_{in} = 200\text{mV}$ in accordance with the Figure 3.5 legend.

As can be seen in Figure 3.5b, the gain response of the driver with the second version of the AB output stage was significantly improved, over the previous version results, shown in Figure 3.5a. The voltage gain was improved, with the second version presenting now a close to unity gain, which contrasts with the much lower gain presented by the first version which was around 0.20 or -14dB. Both systems show a BW over 10MHz.

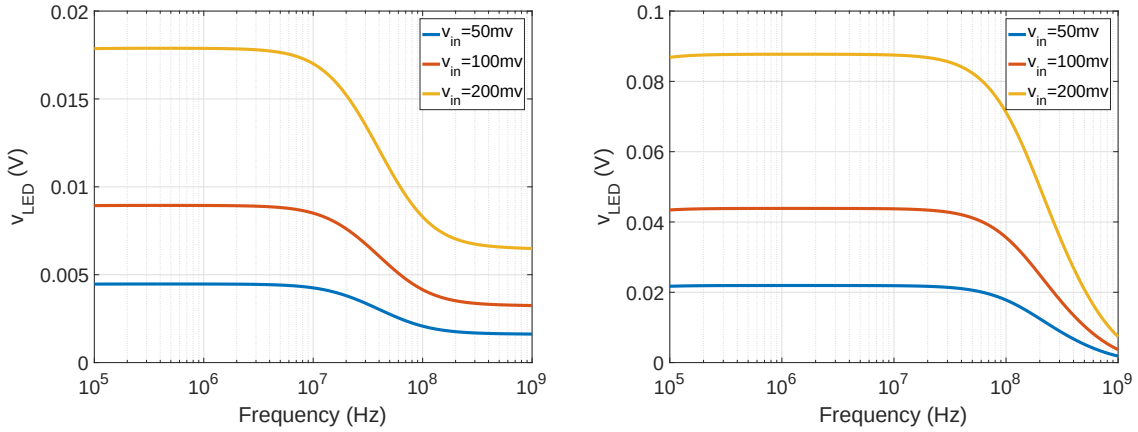

(a) AB first version simulation results **(b)** AB second version simulation results

Figure 3.5: Simulation results for class AB output stage

Figure 3.6 shows the evolutions curve of the total gain for each projected output stage system. Here it is clear to see the voltage gain of the second version of output stage has a gain close to 0dB for all input signal amplitudes, contrasting with the -15db of the first version of the output stage. It is also possible to see an increase of BW, which is now closer to 100MHz BW, this is possible due to the properties of the transistors used for the second version which presented a higher f_T.

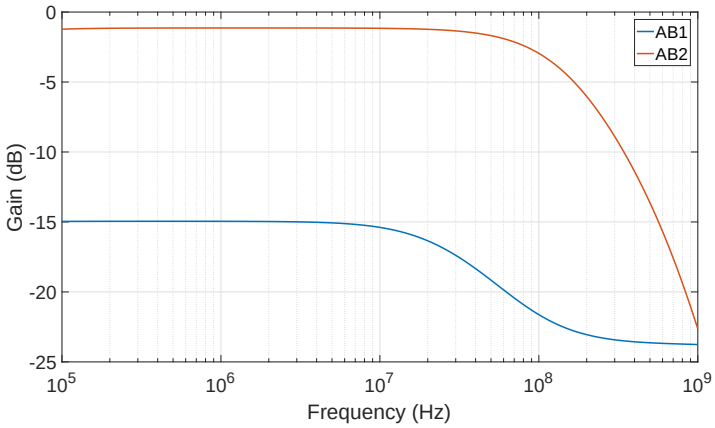

Figure 3.6: Simulation gain results for class AB output stage

3.1.3 Pre-emphasis

The pre-emphasis was designed to act not only for boosting higher frequencies but to also act as a preamplifier for the first version of the class AB output stage. This meant that it should be able to compensate the pole created in the optical power of the LED, and the attenuation of the output stage. To establish a realistic goal the pre-emphasis will be designed to compensate the system at least for one frequency decade, from 3MHz to 30MHz, this is why we will be observing frequencies between 1MHz and 100MHz expecting the experimental system to be able to compensate at least to 30MHz.

For this purpose a three stage amplifier was designed, which the schematic for this circuit can be seen in Figure 3.7, with two stages composed of 'BFR92A',Q1 and Q2, mounted in common emitter configuration, with capacitors, C2 and resistor R12 controlling the signal voltage constant gain, and C4 on the emitter to bypass the emitter resistor and increase the voltage gain by 20db/Dec, creating this way the zero at the required frequency to counteract the optical pole, and the attenuation of the system formed by the AB output stage and the LED. The final stage is a 'BFR92A' in common collector configuration in order to lower the output impedance and provide current gain. The system was biased using a unipolar power supply of +10V.

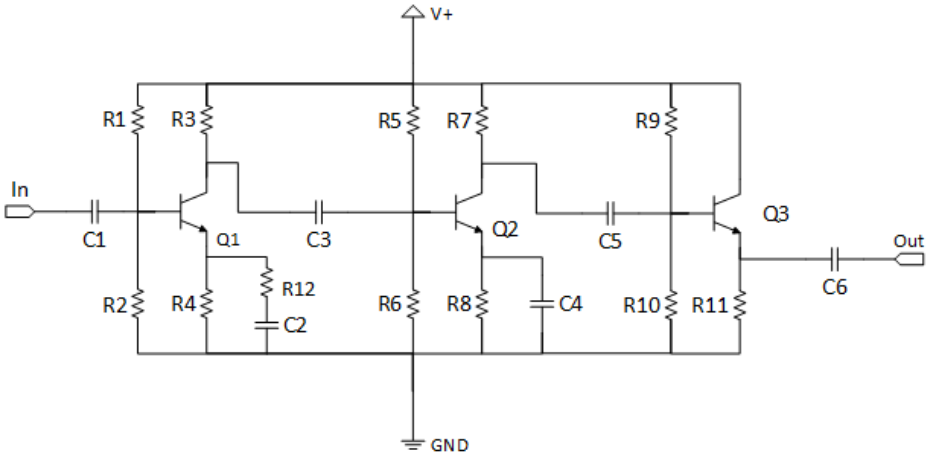

Figure 3.7: Pre-emphasis stage first version schematic

The gain for the two first stages is obtained with the help of the small signal 'π' model of Figure 3.4 and is given by the following equation.

$$A_v = -\frac{gm(R_C \parallel R_L)}{1 + gmR_E} \approx -\frac{R_C}{R_E} \tag{3.4}$$

Note that the gain changes with frequency by influence of the bypass capacitor C4 in the emitter of the second stage formed by Q2. It works as a high-pass filter with a corner frequency F_c given by the following equation, with R_{bypass} being the total impedance in parallel with

the capacitor, and C2 and C4 the bypass capacitors for stage one and two respectively.

$$F_{corner} = -\frac{1}{2\pi R_{bypass} C_{bypass}} \tag{3.5}$$

The gain for the last stage is given by the following equation, and is obtained according to the small signal 'T' model of Figure 3.2.

$$A_{v3} = \frac{gmR_E}{gmR_E + 1} \approx 1 \quad if \quad gmR_E \gg 1 \tag{3.6}$$

The first gain stage was designed to have constant gain of 4 within our working frequency range in case it was connected to the first version of the class AB output stage, so it could counter act the attenuation of 0.25 of the output stage. This gain was controlled by the capacitor C2 and resistor R12, which can be removed to connect the pre-emphasis system to the second version of the output stage with its own pre-amplifier, and turning the first stage formed by Q1 in a unity gain stage. The second gain stage was designed to be the originator of the desired zero to counter act the optical pole, with the frequency at which it occurs controlled by C4. Table 3.3 gives us the values for the components used in this system.

Table 3.3: Pre-emphasis component values

Component	**Value/Model**	**Component**	**Value/Model**	**Component**	**Value/Model**
R1	$4k\Omega$	R11	150Ω	V+	10V
R2	$4k\Omega$	C1	10μF	-	-
R3	550Ω	C2	10μF	-	-
R4	370Ω	C3	10μF	-	-
R5	$4k\Omega$	C4	150pF	-	-
R6	$4k\Omega$	C5	10μF	-	-
R7	550Ω	C6	10μF	-	-
R8	370Ω	Q1	BFR92A	-	-
R9	$5k8\Omega$	Q2	BFR92A	-	-
R10	$2k2\Omega$	Q3	BFR92A	-	-

As it is clear to see from the results of the simulations in Figure 3.8a and Figure 3.8a, which present us with the voltage applied to the LED in the first case for the pre-emphasis connected in series with the first version of the AB output stage, and in the second case for the pre-emphasis connected to the second version of the AB output stage. Both systems now are able to present a unity voltage gain with an inversion of phase, for lower working frequencies, and the the 3dB gain frequency is now located at approximately 10MHz for the first version and 100MHz for the second version. The evolution of the gain versus frequency is presented in Figure 3.6.

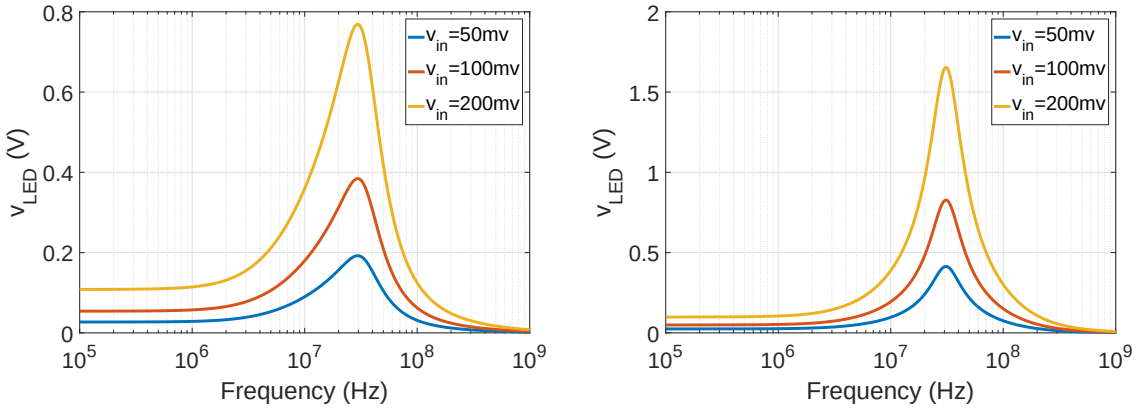

(a) AB first version **(b)** AB second version

Figure 3.8: Simulation voltage results for class AB output stage with pre-emphasis

In Figure 3.9 we can observe an evolution for the gain of 20dB/Dec for both systems until the maximum possible gain level is reached, after that the natural pole of the output stage becomes dominant, and the gain will follow the response of the full system lowering the gain level -20dB/Dec.

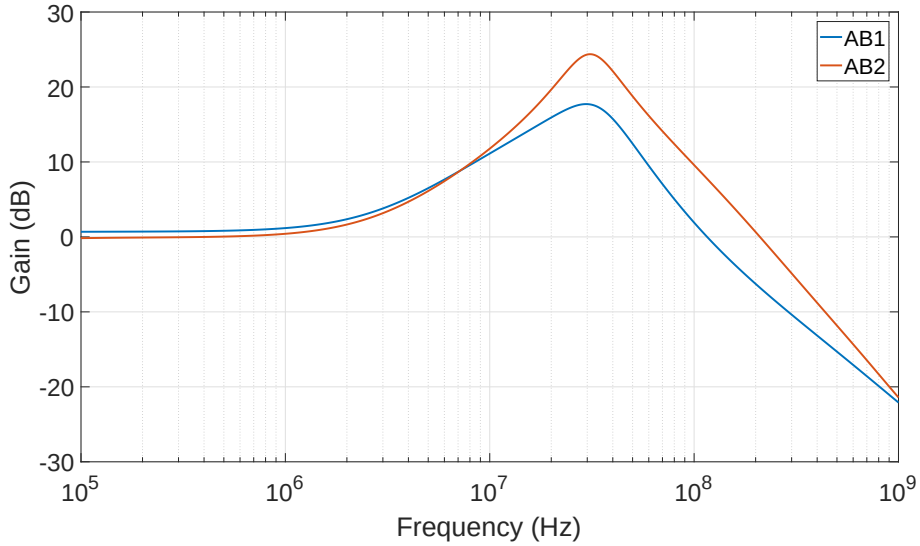

Figure 3.9: Simulation gain results for class AB output stage with pre-emphasis

According to these results it is expected that these systems will be able to counteract the optical pole caused by the LED and extend its BW beyond its original 3MHz. The optical response of the implemented system is expected now to remain close to flat until the maximum gain of the system is reached, when it will start to also be affected by the driving system pole, and should present a descending curve of about -40dB/Dec caused by the two poles it is now subjected to, the optical one that started at 3MHz, and the electrical one which is expected to be around 100MHz.

3.2 Receiver design

For testing purposes a simple receiver design was built based on the recommended schematics of the data sheet of the PD, supplied by the manufacturer, which can be seen on Figure 3.10. The PD was biased with an external power supply of +20V, and a R_L of 50Ω was chosen.

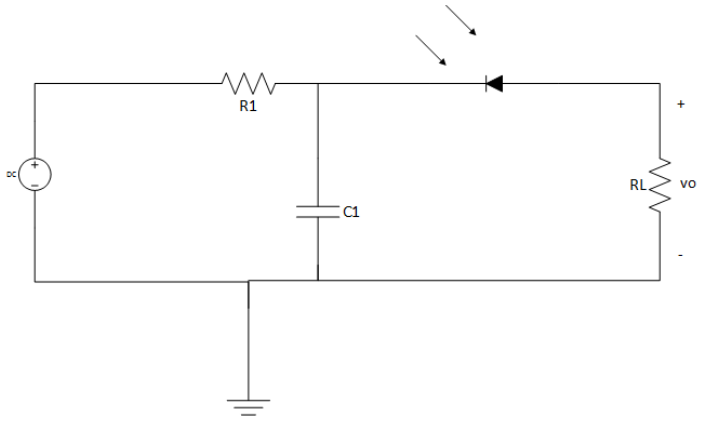

Figure 3.10: PD schematic [22]

The incident optical power relation with voltage is given by.

$$v_o = P_{optical} \times \Re(\lambda) \times R_L \tag{3.7}$$

With $\Re(\lambda)$ being the spectral responsibility, which can be seen in Figure 3.11.

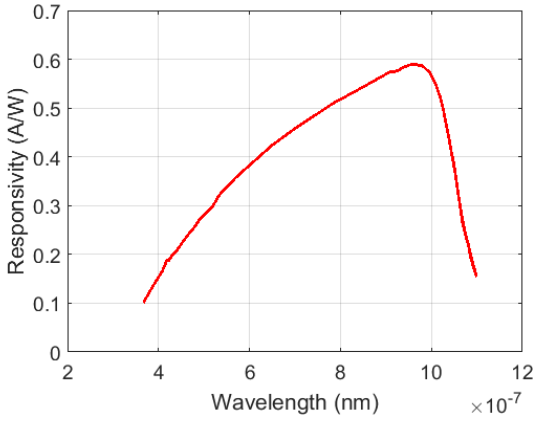

Figure 3.11: FDS100 responsivity curve [22]

The BW given by.

$$f_{BW} = \frac{1}{2\pi R_L C_J} \tag{3.8}$$

And the rise time.

$$t_R = \frac{0.35}{f_{BW}} \tag{3.9}$$

CHAPTER 4

Implementation and Results

4.1 LED characterization

The LED luminous power follows the curve supplied in the manufacturers data sheet, similar to the one in figure 4.1, that shows how electrical current relates to its relative luminous power. This permits us to find a working zone for the electrical current as close to linear as possible. From Figure 4.1 we can observe that the manufacturer normalized the relative luminous flux to 350mA, which is located in a close to linear operating region, this value will be considered as our biasing current around which the tests in this section will be conducted.

The LED will be the load of our driving circuit, this means that some parameters must be determined in order for it to be operated in a linear region and with the desired median luminous flux. Some of these parameters can be obtained via the manufacturer data sheet, others are not given by the manufacturer and must be obtained by measuring the LED response. Such is the case with the LED BW, AC and DC impedance that must be measured by experimental means which is done in this chapter.

Given that operating LEDs produce a lot of heat, some construction methods for the mounting PCB of the LED will be evaluated for their heat sinking capabilities.

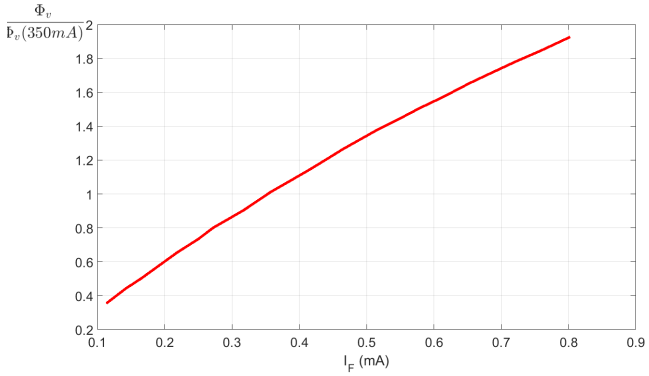

Figure 4.1: Osram Oslon SSl 80 Relative luminous flux

4.1.1 LED Thermal Analysis

A study of the LED thermal behaviour was conducted in order to establish an efficient heat dissipation method to use. For this purpose two Printed Circuit Board (PCB) were designed. The first one as a more simple approach, lacked the appropriate heat sinking footprint, but was the largest of the two Figure 4.2a. The second, with a more advanced design to improve heat sink, was significantly smaller than the first Figure 4.2b. This designed was based on the recommended footprint provided by the manufacturer but with some alterations intended to improve the thermal efficiency. While the recommended design only used two parallel copper lanes connected at the middle through the LED thermal pad, we decided to enlarge the copper lanes outward in triangular shape and drill holes to pass vias to the bottom side of the PCB where a copper negative of the top design was routed. This is a common practice to improve heat sink when dealing with HB LEDs, and the idea is to increase the surface area exposed to air.

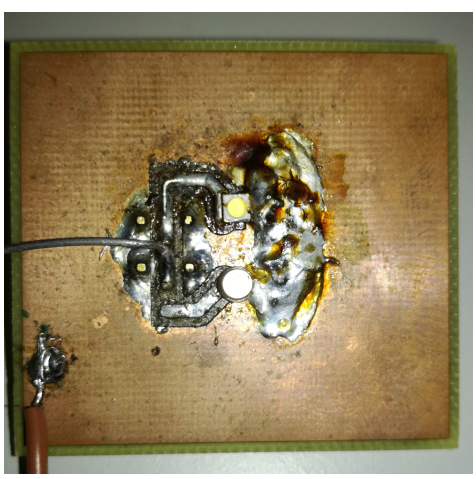

(a) LED PCB 1

(b) LED PCB 2

Figure 4.2: Implemented LED PCBs

The study of these two PCB heat sinking behaviour showed that the benefits of a more adequate heat dissipation footprint was not enough to counteract the impact of a smaller overall size of the mounting PCB. This can be seen on the thermal images of Figure 4.3a and Figure 4.3b, where both the LEDs are biased with the same forward current of 350mA, and PCB 1 shows a lower temperature value compared to PCB2. Figure 4.4 shows the evolution of temperature according to current 4.4a, and power 4.4b, and as it can be seen for higher current values, above 400mA, the difference in temperature between the two PCBs increases to a point where at 700mA PCB2 reaches the maximum temperature rating of the LED of 120 °C while the PCB1 is 105 °C.

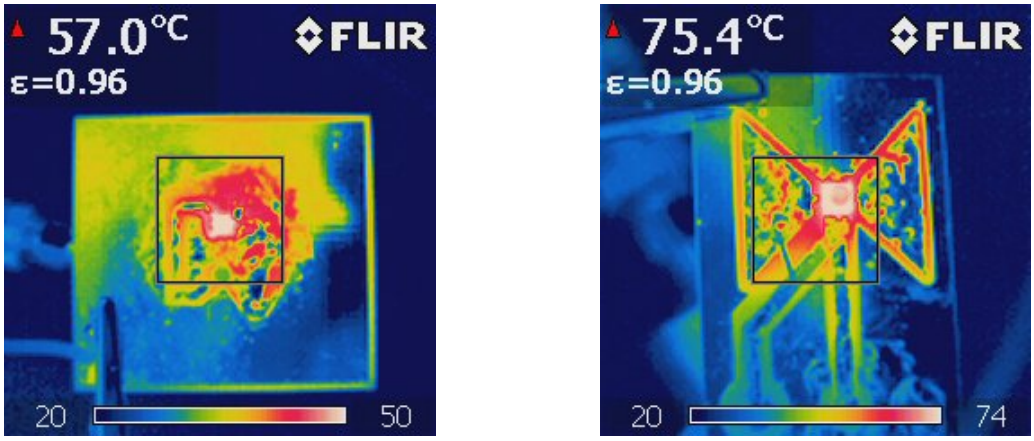

(a) LED PCB 1 IR thermal camera image @ 350mA

(b) LED PCB 2 IR thermal camera image @ 350mA

Figure 4.3: LED PCB's Thermal images

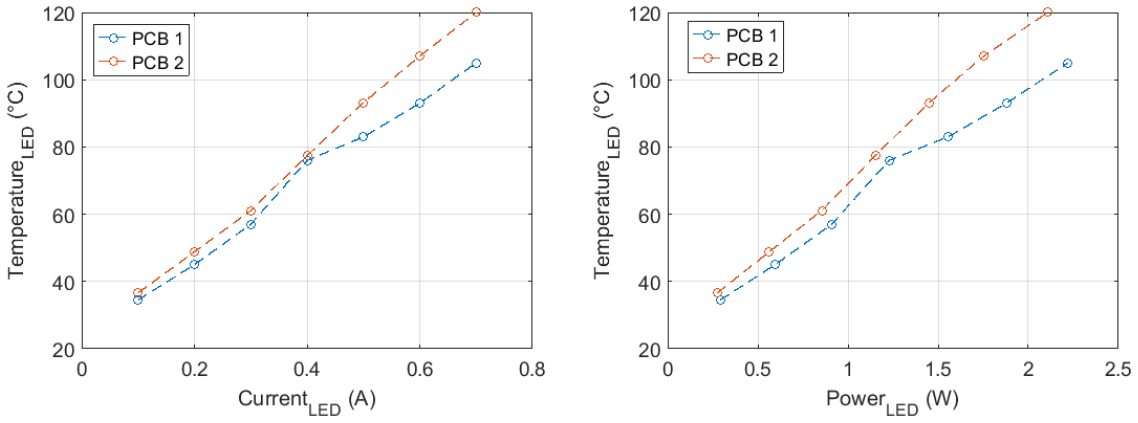

(a) LED Temperature vs. forward current

(b) LED Temperature vs. power

Figure 4.4: LED temperature measures

4.1.2 LED DC Analysis

For the DC analysis, a voltage was applied to the LED in series with a 10Ω resistor. The voltage was measured directly from the LED and the current was calculated using the biasing resistor. Figure 4.5a shows the evolution of DC current versus the DC voltage of the LED, the divergence from the data sheet values can be explained by the difference in heat dissipation efficiency, since PCB2 was the one with lowest heat sinking capabilities the current rises faster than PCB1. With these values the DC impedance was obtained as shown in Figure 4.5b versus the current, and here we can conclude the value of the DC impedance to be around 8Ω for 350mA. Also obtained from these measurements, we have the LED forward current versus total DC power Figure 4.5c, where we can conclude the total power of the LED for a forward current biasing of 350mA to be around 1W.

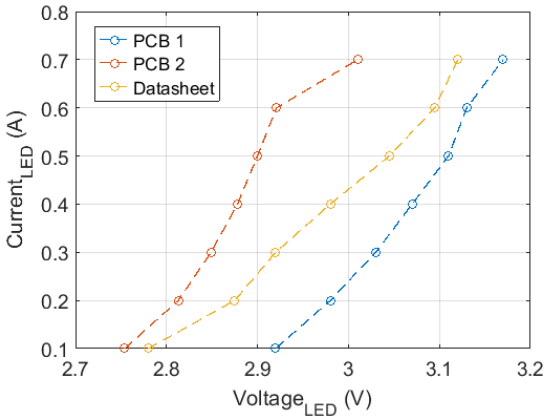

(a) LED V-I curve

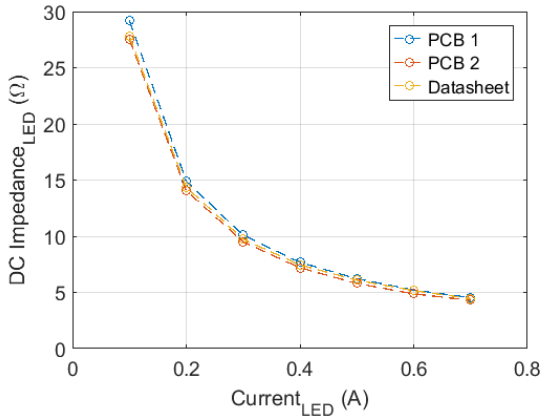

(b) LED DC impedance vs. current

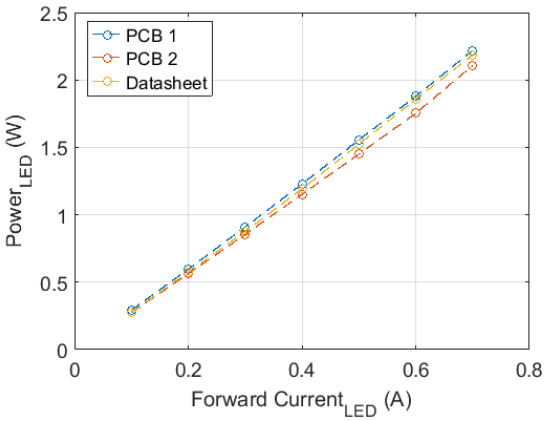

(c) LED DC power vs. current

Figure 4.5: LED PCB's DC Analysis

4.1.3 LED AC Analysis

LED AC Impedance

To determine the the LED AC impedance, pairs of voltage and current variation were measured. The current was measured through a resistor connected in series with the LED, and the voltage directly on the LED.

These measurements were taken with the LED biased at specific DC current biasing points, that were controlled by a DC power supply. These values for DC biasing current were centered in the desired 350mA, and with variation of minus and plus 50mA, yielding respectively 300mA and 400mA. Two signal mixing techniques were used for biasing the LED and mixing the modulating voltage. In one method this was accomplished by using a Bias-T that decoupled the DC current and AC signal. The other method consisted of a 10Ω resistor in series with a DC power source and the LED, and a 10μF capacitor that was used to keep the DC current from flowing to the source.

For the LED impedance measurement a 0.16Ω resistor was connected in series with the LED after the Bias-T or the capacitor according to the situation (Figure 4.6). Voltage measurements were then done to the terminals of this resistor to determine the impedance of

the LED.

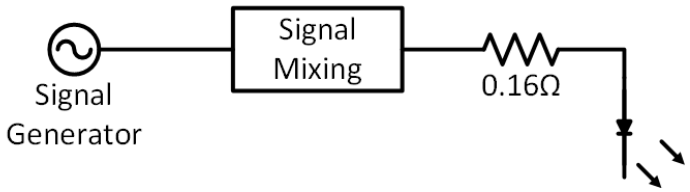

Figure 4.6: Experimental measurement setup for LED impedance

Figure 4.7 shows the results of the input impedance measurements done for the LED with both signal mixing techniques. Though some divergence in values can be observed for 100MHz, the impedance value of the LED remains fairly constant until 50MHz which is within our range of interest.

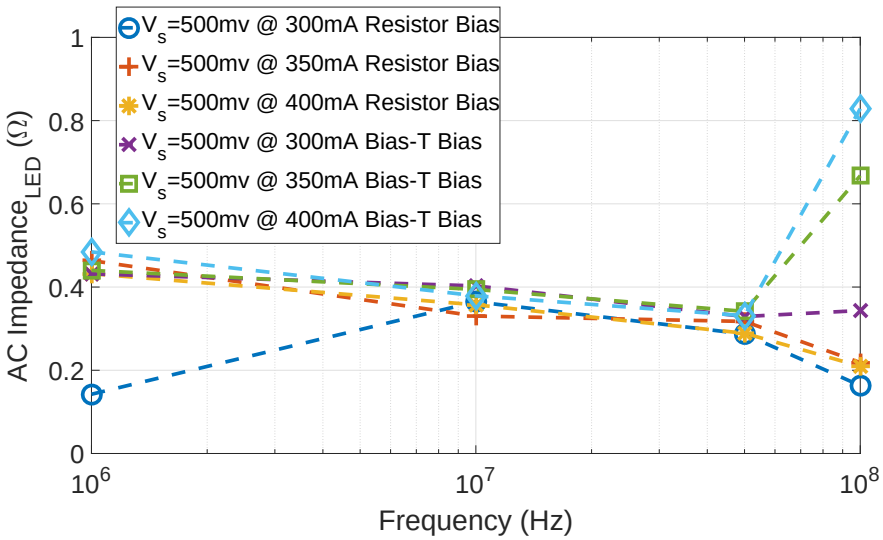

Figure 4.7: LED AC impedance

The values of input impedance shown by the Bias-T and the 10μF capacitor were also measured. The Device Under Test (DUT) was operated by a signal generator with an output impedance of 50Ω, and both measurements were made with the use of a 4.7Ω resistor in series between the signal generator and the DUT, upon which voltage measurements of both terminals were made for input impedance calculation purposes (Figure 4.8).

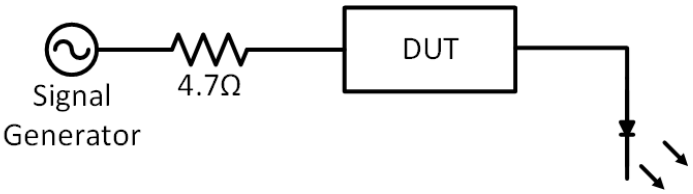

Figure 4.8: Experimental measurement setup for signal mixing method input impedance

The results present in Figure 4.9 for the two different signal mixing methods showed no significant difference between the two regarding the AC input impedance of mixing signal

device. They are also in accordance with the LED impedance values, suggesting both methods are transparent for the signal and should not influence the signal.

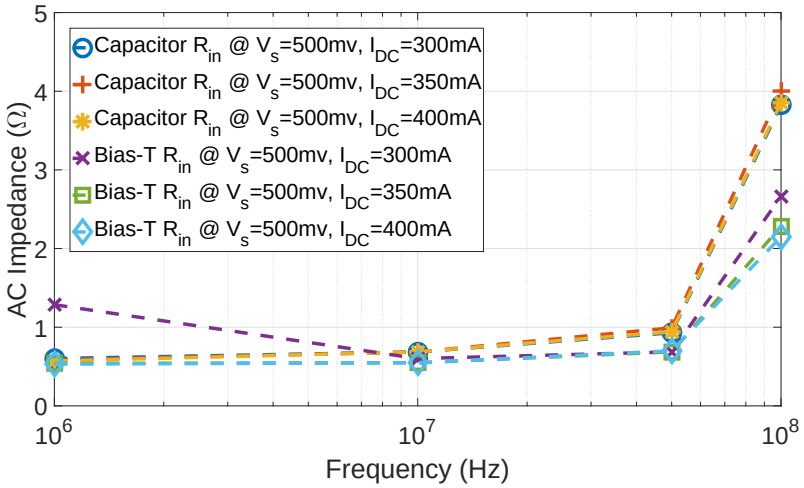

Figure 4.9: Bias-T and 10μF Capacitor AC input impedance

LED BW

To establish the optical BW of the LED, measurements were made with the help of the test receiver system. The emitter and receiver systems were placed approximately 2cm apart, the LED was biased with a current of 350mA, and then voltage measurements were taken, both on the LED and the PD. This information was used to calculate the optical pole of the system, and then designing the pre-emphasis stage. Figure 4.10 shows the evolution of the signal amplitude versus frequency. As can be seen here, the voltage amplitude of the signal applied to the LED raises when reaching 50MHz, but exhibits fairly constant values below that frequency. Also noticeable is the strong attenuation of 0.04 of the initial signal applied to the driver.

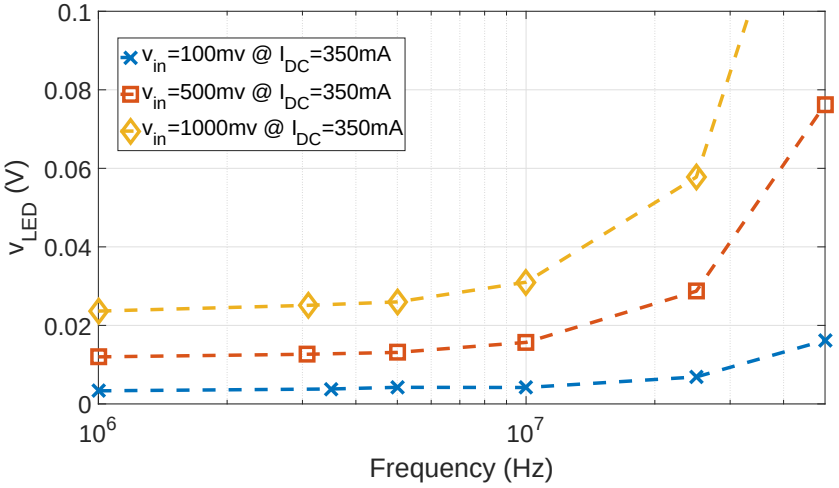

Figure 4.10: LED BW analysis - LED modulating signal

All measurements revealed a significant rise in the amplitude of the signal applied to the LED for higher frequencies (Figure 4.10), however this did not translate into a higher transmitted signal amplitude (Figure 4.11) since the LED shows lower photon emission levels for these higher frequencies.

To calculate the cut-off frequency of the LED we first established the range of frequencies at which we want the system to work on, between 1MHz and 100MHz, then the amplitude of the signal was measured on the receiver side at the lowest working frequency to establish the maximum voltage amplitude. An ascending frequency sweep was made starting at the maximum voltage amplitude frequency, and the received signal was then observed until it became 0.707 of the maximum signal. The frequency at this point was considered to be the cut-off frequency of the LED. As we can see in Figure 4.11, measured cut-off frequencies were consistently found around 3MHz for all measurements, these values were expected for a pc-LED like the one measured.

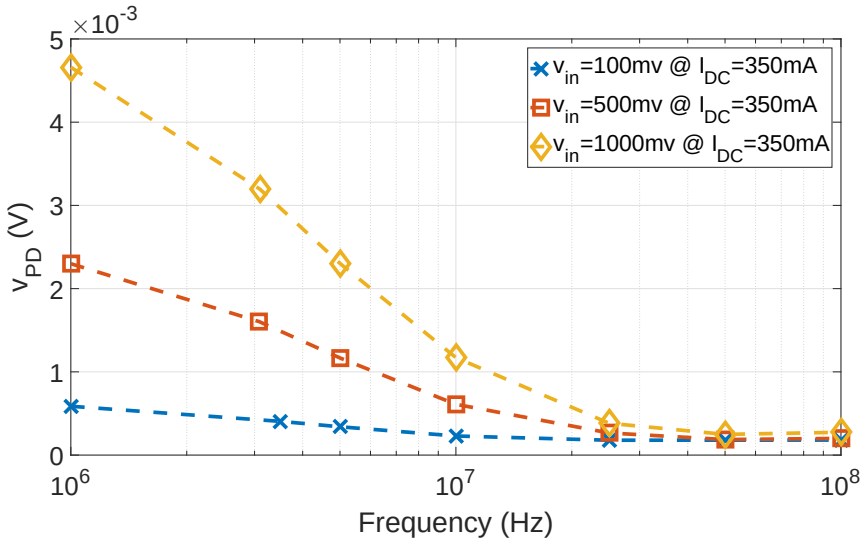

Figure 4.11: LED BW analysis - PD received signal

4.2 Class AB1 output stage analysis

To determine the best biasing approach for the LED, measurements were made with two distinct signal mixing methods just like in section 4.1.3, one using the Bias-T, and another with a 10μF capacitor as a DC block and a 10Ω resistor biasing the LED. The LED was then DC biased at 350mA and an AC source generated a continuous sinusoidal signal that was injected on the LED. Voltage measurements were done directly on the LED on the emitter side, and on the load impedance R_L (Figure 3.10) of the receiver system. The developed PCB used in this section is presented in figure 4.12, and it follows the schematic presented in section 3.1.1 Figure 3.1.

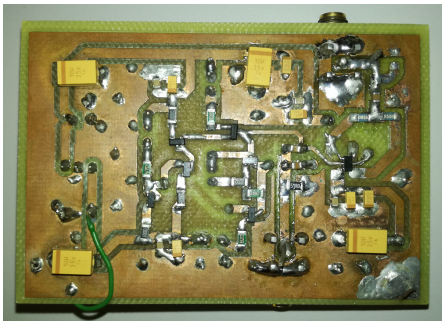

(a) First version of the class AB output stage PCB top view

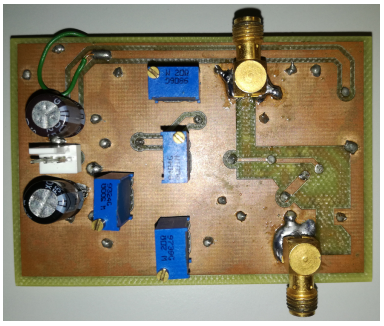

(b) First version of the class AB output stage PCB bottom view

Figure 4.12: First version of the class AB output stage PCB

4.2.1 Frequency response analysis

Resistor Biasing

Figure 4.13 shows the voltage amplitude of the signal applied to the LED for three different input amplitude signals, V_{in} = 50mV, V_{in} = 100mV, and V_{in} = 200mV, these values were chosen based on system stability, since higher amplitude signals caused the output transistor to handle very high power values of about 700mw which in turn caused the output transistors Q2 and Q3 (Figure 3.1) to overheat and saturate, rendering the system nonoperational. This showed the importance of an adequate heat sinking design for the output stage formed by Q2 and Q3, and it is caused by the very low AC impedance value of the LED, which as seen on Figure 4.7 is always smaller than 1Ω for our working frequency range, and will draw high current values. For these measurements the LED was biased with a current of 350mA.

The voltage modulation signal values now applied to the LED with the AB output stage are higher (Figure 4.13) for the same amplitude signal levels of the signal generator than those of the values directly applied with the signal generator to the LED (Figure 4.10), but still suffer an initial attenuation of around 0.35 since the driver although being capable of delivering some gain, it is not enough to reach unity gain for the full system. Also noticeable in Figure 4.13 is the presence of a pole which leads to a decay of around -20dB (Figure 4.14) in the first decade, that was not present on the measures of Figure 4.10 nor the simulations.

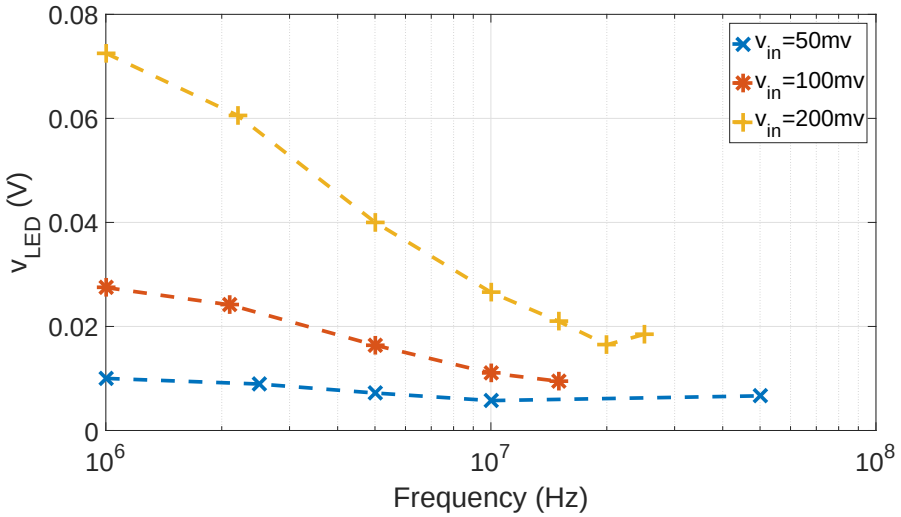

Figure 4.13: First version AB output stage BW analysis - LED signal voltage

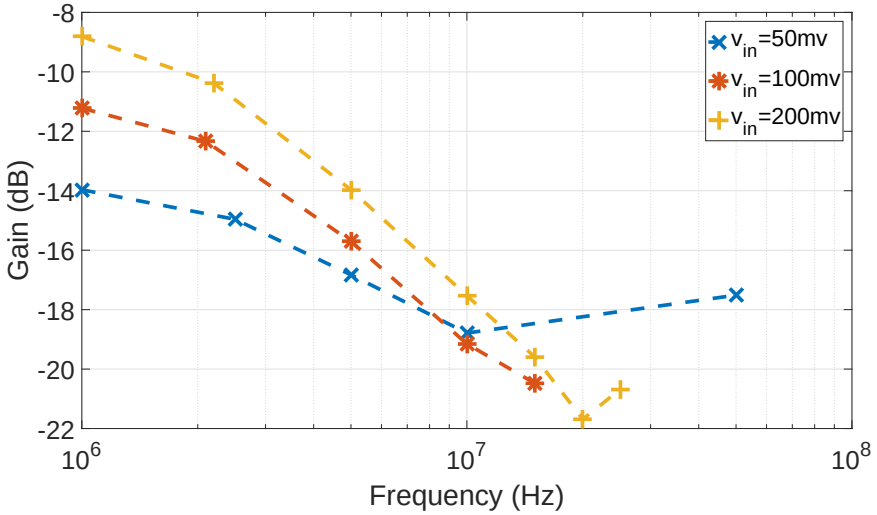

Figure 4.14: First version AB output stage BW analysis - System signal gain

Figure 4.15 shows the voltage amplitude of the received signal on the PD R_L (Figure 3.10), with these values the -3dB BW of the system was determined when the amplitude of the signal at the starting frequency of 1MHz was reduced to 0.707 of its value. The signal amplitude evolution curve of Figure 4.15 reveals a fall of -40dB on the first decade which contrast with the -20dB fall seen on Figure 4.11 and reveals the second pole introduced with the AB output stage. However the overall received signal levels are now also higher than the PD received signals without the AB output stage of Figure 4.11, has was expected because of the higher modulation levels applied to the LED (Figure 4.13).

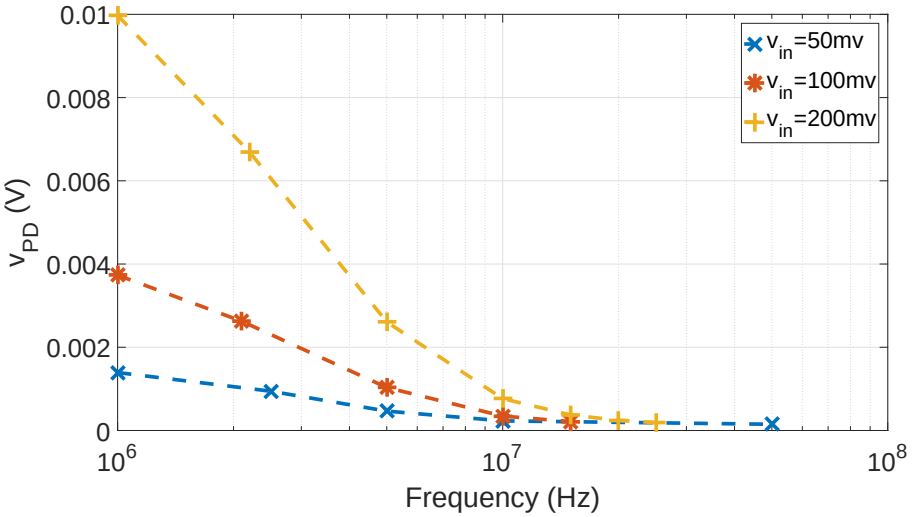

Figure 4.15: First version AB output stage BW analysis - PD received signal voltage

Bias-T Biasing

Figure 4.16 shows the measuring results for the the voltage applied to the LED by the Bias-T biasing method, that were conducted in the same way has before with the same input amplitude signals, $V_{in} = 50\text{mV}$, $V_{in} = 100\text{mV}$, and $V_{in} = 200\text{mV}$. Has can be seen, the behaviour of the system did not show significant differences over the biasing method, with the signal voltage amplitude applied to the LED remaining similar as for the resistor biasing method.

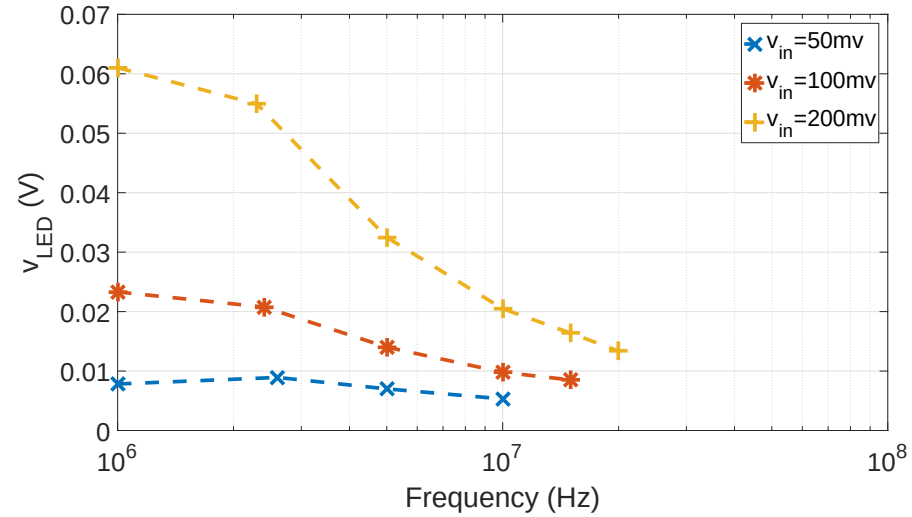

Figure 4.16: First version AB output stage BW analysis - LED signal voltage

The gain of the system also remained similar in both approaches (Figure 4.17). This led us to conclude that both biasing methods were effective, and efficiency or simplicity were the main choosing factors for signal mixing method.

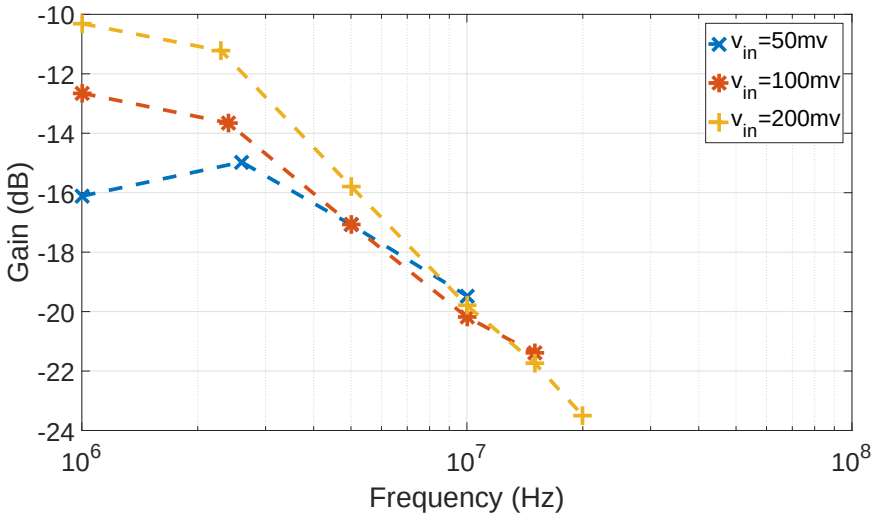

Figure 4.17: First version AB output stage BW analysis - System signal gain

Figure 4.18 shows the received signal voltage amplitude, and as expected the results are similar to the ones in Figure 4.15.

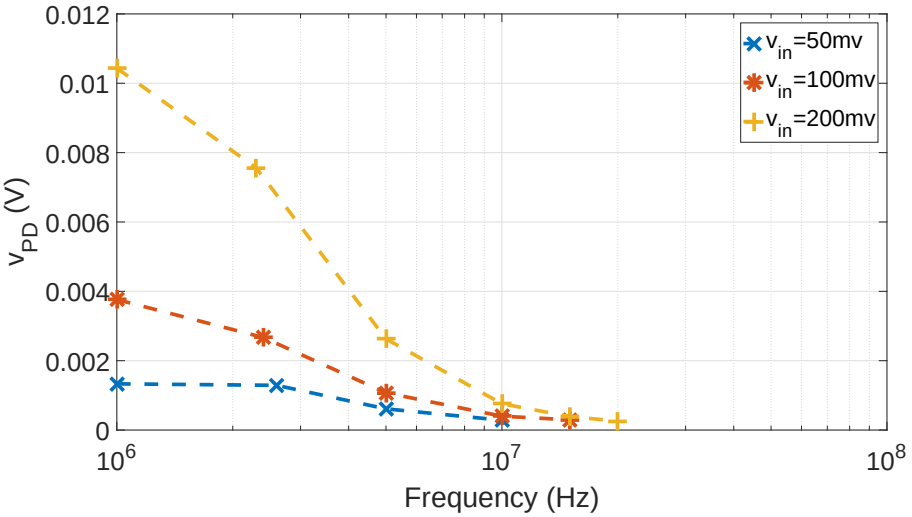

Figure 4.18: First version AB output stage BW analysis - PD received signal voltage

4.3 Class AB2 output stage analysis

A similar study to the first class AB output stage was planned, with the same type of tests being made, but due to late arrival of the needed components such analysis was not possible.

4.4 Pre-emphasis stage analysis

The pre-emphasis implementation proved to be effective in counteracting the system pole to some extent. However this simple design, which only accounted for the zeros of the system without concern for the new poles introduced, rendered the system unstable for higher input

signals, as the gain would increase to the point of saturation if gain limiting methods were implemented. The developed PCB used in this section is presented in figure 4.19.

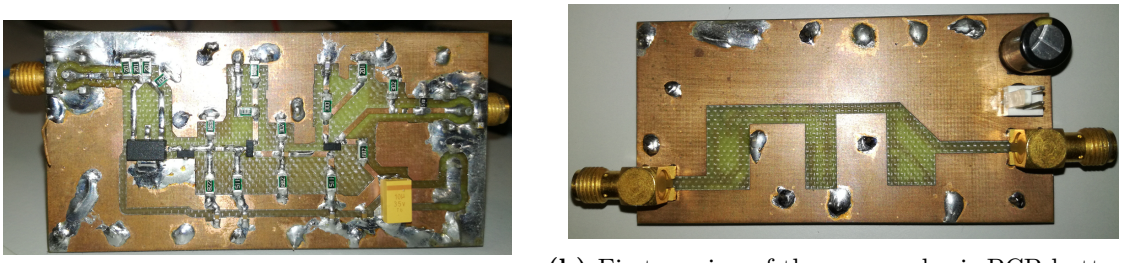

(a) First version of the pre-emphasis PCB top view

(b) First version of the pre-emphasis PCB bottom view

Figure 4.19: First version of the pre-emphasis PCB

Figure 4.20 shows the results of a Fast Fourier Transform (FFT) analysis of the implemented pre-emphasis circuit. This measurement was done by connecting a 50Ω load to the output of the circuit and short circuiting the input to the reference ground. Here it is clear to see a spike at around 240MHz, this spike represents the measured the natural oscillation of this circuit reaching around -20dB. This oscillation can be attributed to the high gain levels for higher frequencies caused by the pre-emphasis, which when combined with an inadequate design that may have lead to positive feedback loops, caused this very high amplitude oscillation that rendered this system incapable of delivering the signal without introducing high levels of noise, which is unacceptable for a good performance driver.

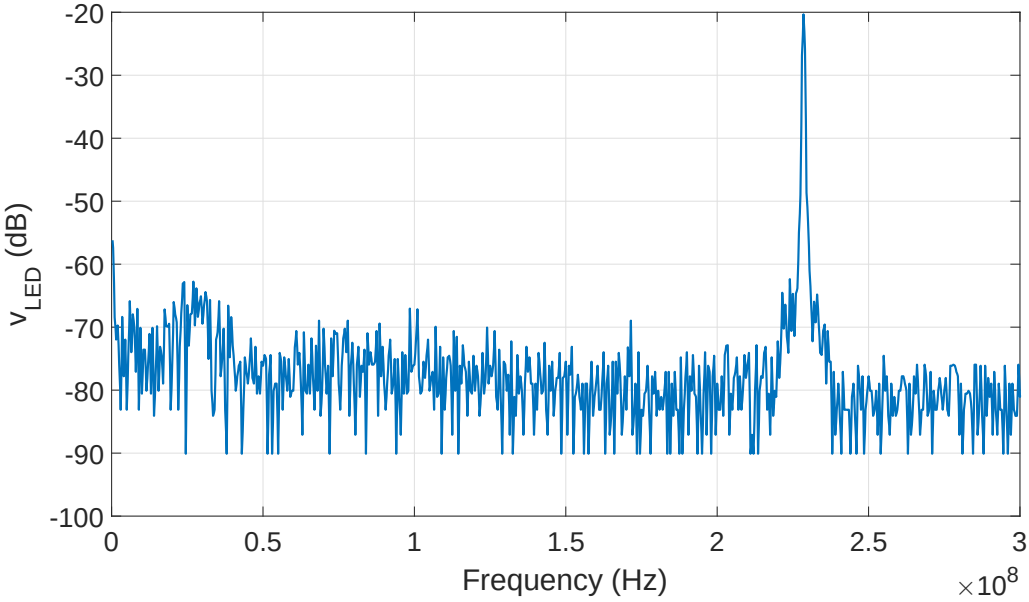

Figure 4.20: No signal pre-emphasis FFT

CHAPTER 5

Conclusion

5.1 Conclusions

The main objective of this dissertation was to design an effective driver for VLC analog signal transmission.

In chapter 2 the state of the art study provided the necessary basis for the design of the driver, since the design is based on previously validated design methods for VLC drivers.

In chapter 3 all the designs were simulated in order to get a realistic vision of the system behaviour.

In Chapter 4 the developed practical PCB circuits are shown, and so are the possible results, for temperature and system response. Not all desired measurements were possible, due to time constrains or due to physical circuits issues. Here we can conclude that the LED dynamic impedance was found to be of a small magnitude appearing to be smaller than 1Ω within the range of frequencies for which we conducted our study. Also was concluded that an efficient heat sink design may help to improve the LED lifetime. The selection of transistors for the output stage proved to be a difficult task, asking for high power rated transistors to be used, with efficient heat sinking and additional air cooling. The pre-emphasis design was found capable of improving the systems BW to a certain level, but gain limitation for higher frequencies are essential to prevent frequency components out of working range to be amplified to a level at which will affect the signal.

5.2 Future Work

The use of post-equalization on the receiver side will help improve the overall system BW. This would permit the driving circuit to perform under lower gains thus improving its power and thermal efficiency. The work load would be shared by both front ends of the system.

References

[1] M. Wolf, L. Grobe, J. Vucic, D. O. Brien, O. Bouchet, H. L. Minh, G. Faulkner, J. Li, J. W. Walewski, S. Nerreter, K.-d. Langer, E. Gueutier, and P. Porcon, "SEVENTH FRAMEWORK PROGRAMME THEME 3 Information & Communication Technologies (ICT) OMEGA Physical Layer Design and Specification", 2010.

[2] S. Kyatam, P. Camacho, L. Rodrigues, L. N. Alves, and J. C. Mendes, "Thermal analysis of high power light emitting diodes using diamond layered pcb", European Conference on Circuit Theory and Design, Catania, Italy, May 2017.

[3] S. Kyatam, P. Camacho, L. Rodrigues, L. N. Alves, and J. C. Mendes, "Thermal analysis of high power leds", Workshop on Compound Semiconductor Devices and Integrated Circuits held in Europe, Las Palmas, Spain, Sep. 2017.

[4] X. Huang, X. Gao, and Z. Yan, "Security protocols in body sensor networks using visible light communications", *International Journal of Communication Systems*, 2015.

[5] K. Qiu, F. Zhang, and M. Liu, "Let the light guide us: Vlc-based localization", *IEEE Robotics & Automation Magazine*, vol. 23, no. 4, pp. 174–183, 2016.

[6] A. G. Bell, W. G. Adams, Tyndall, and W. H. Preece, "The photophone and the conversion of radiant energy into sound", *Telegraph Engineers, Journal of the Society of*, vol. 9, no. 34, pp. 375–383, 1880. DOI: 10.1049/jste-1.1880.0044.

[7] L. U. Khan, "Visible light communication: Applications, architecture, standardization and research challenges", *Digital Communications and Networks*, 2016.

[8] G. Pang, T. Kwan, C.-H. Chan, and H. Liu, "Led traffic light as a communications device", in *Intelligent Transportation Systems, 1999. Proceedings. 1999 IEEE/IEEJ/JSAI International Conference on*, IEEE, 1999, pp. 788–793.

[9] E. F. Schubert, T. Gessmann, and J. K. Kim, *Light emitting diodes*. Wiley Online Library, 2005.

[10] H. Welker, *Semiconductor devices and methods of their manufacture*, US Patent 2,798,989, Jul. 1957. [Online]. Available: https://www.google.com/patents/US2798989.

[11] R. N. Hall, G. E. Fenner, J. D. Kingsley, T. J. Soltys, and R. O. Carlson, "Coherent light emission from gaas junctions", *Phys. Rev. Lett.*, vol. 9, pp. 366–368, 9 Nov. 1962. DOI: 10.1103/PhysRevLett.9.366. [Online]. Available: https://link.aps.org/doi/10.1103/PhysRevLett.9.366.

[12] H. Rupprecht, J. M. Woodall, K. Konnerth, and D. G. Pettit, "Efficient electroluminescence from gaas diodes at 300°k", *Applied Physics Letters*, vol. 9, no. 6, pp. 221–223, 1966. DOI: 10.1063/1.1754721. [Online]. Available: http://dx.doi.org/10.1063/1.1754721.

[13] S. Z. Zabih Ghassemlooy Luis Nero Alves and M.-A. Khalighi, *Visible Light Communications: Theory and Applications*. CRC Press, Jun. 2017, ch. 2, ISBN: 9781498767538.

[14] D. Karunatilaka, F. Zafar, V. Kalavally, and R. Parthiban, "LED Based Indoor Visible Light Communications: State of the Art", *IEEE Communications Surveys & Tutorials*, vol. 17, no. 3, 1649–1678, 2015, ISSN: 1553-877X. DOI: 10.1109/COMST.2015.2417576. [Online]. Available: http://ieeexplore.ieee.org/lpdocs/epic03/wrapper.htm?arnumber=7072557.

[15] G. Xiaoyun, J. Graff, and E. Schubert, "Photon recycling semiconductor light emitting diode.", *International Electron Devices Meeting 1999 Technical Digest (Cat No99CH36318)*, p. 600, 1999, ISSN: 9780780354104.

[16] S. B. Alexander, *Optical communication receiver design*. SPIE Press, 1997, vol. 37.

[17] A. M. Khalid, G. Cossu, R. Corsini, P. Choudhury, and E. Ciaramella, "1-Gb/s transmission over a phosphorescent white LED by using rate-adaptive discrete multitone modulation", *IEEE Photonics Journal*, vol. 4, no. 5, pp. 1465–1473, 2012, ISSN: 19430655. DOI: 10.1109/JPHOT.2012.2210397.

[18] S. Hranilovic, *Wireless optical communication systems*. Springer Science & Business Media, 2006.

[19] A. S. Sedra and K. C. Smith, *Microelectronic circuits*. New York: Oxford University Press, 1998, vol. 1.

[20] H. Li, Y. Zhang, X. Chen, C. Wu, J. Guo, Z. Gao, W. Pei, and H. Chen, "682 Mbit/s phosphorescent white LED visible light communications utilizing analog equalized 16QAM-OFDM modulation without blue filter", *Optics Communications*, vol. 354, pp. 107–111, 2015. DOI: 10.1016/j.optcom.2015.05.033. [Online]. Available: http://dx.doi.org/10.1016/j.optcom.2015.05.033.

[21] Z. Ghassemlooy, W. Popoola, and S. Rajbhandari, *Optical wireless communications*. CRC Press Boca Raton, FL, 2012.

[22] *Fds100 si photodiode*, 0637-S01, Rev. L, Thorlabs, Feb. 2017.

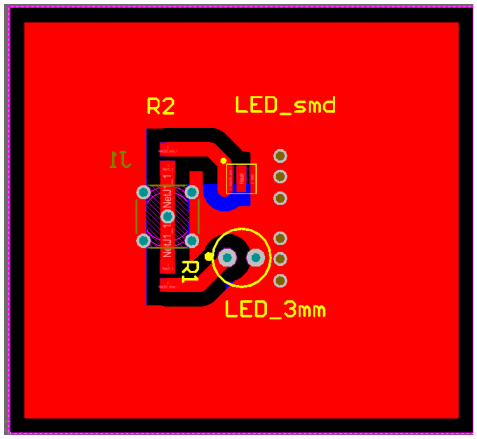

Figure 1: LED PCB1 layout top view

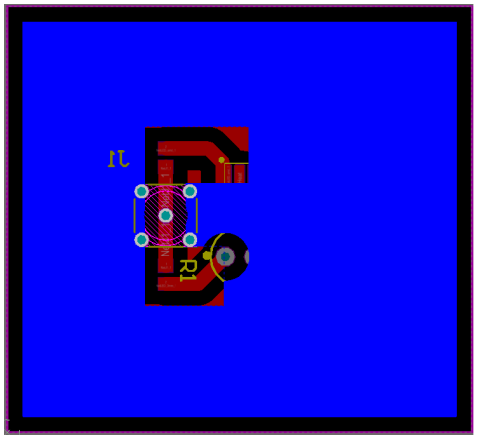

Figure 2: LED PCB1 layout bottom view

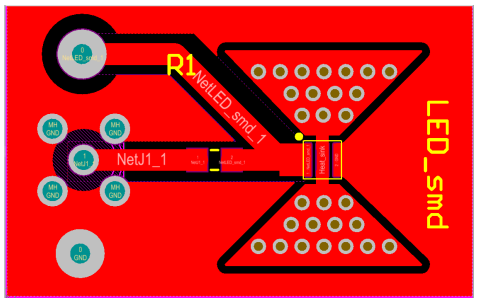

Figure 3: LED PCB2 layout top view

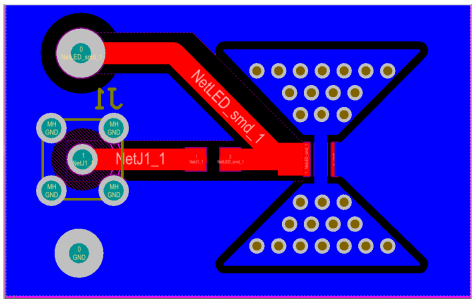

Figure 4: LED PCB2 layout bottom view

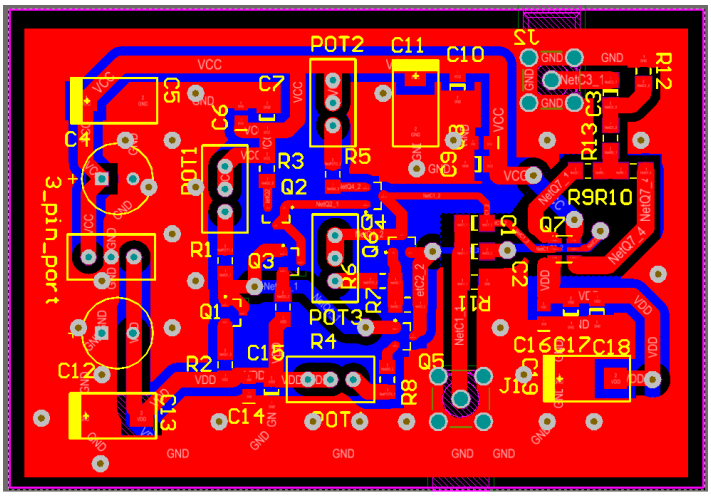

Figure 5: First AB output stage PCB layout top view

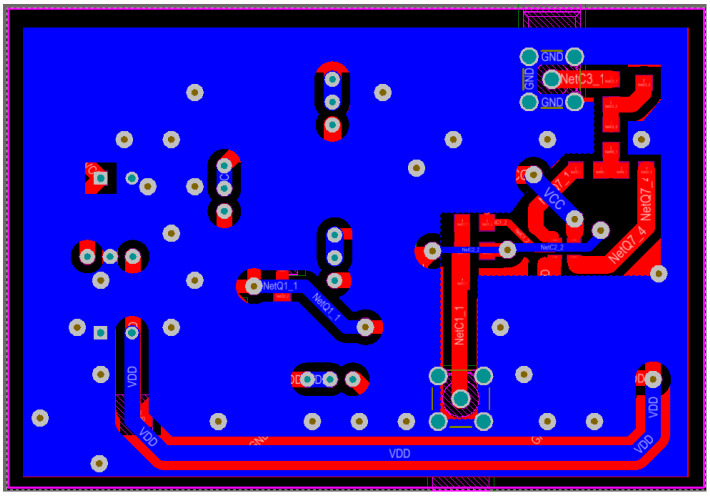

Figure 6: First AB output stage PCB layout bottom view

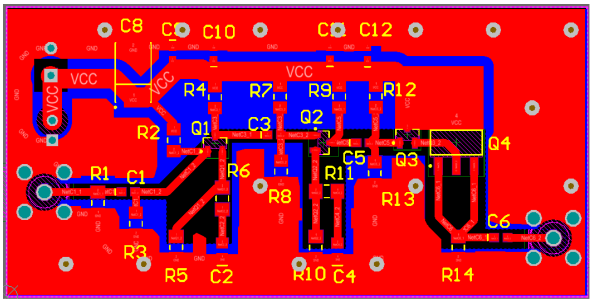

Figure 7: Pre-emphasis stage PCB layout top view

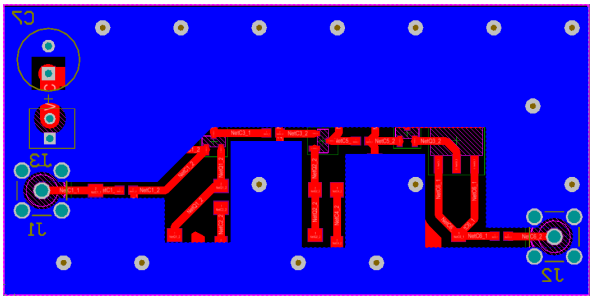

Figure 8: Pre-emphasis stage PCB layout bottom view